Eight Millisecond Pulsars Discovered in the Arecibo PALFA Survey

E. Parent[1], V. M. Kaspi[1], S. M. Ransom[2], P. C. C. Freire[3], A. Brazier[4], F. Camilo[5], S. Chatterjee[4], J. M. Cordes[4], F. Crawford[6], J. S. Deneva[7], R. D. Ferdman[8], J. W. T. Hessels[9,10], J. van Leeuwen[9,10], A. G. Lyne[11], E. C. Madsen[1], M. A. McLaughlin[12,13], C. Patel[1], P. Scholz[14], I. H. Stairs[15], B. W. Stappers[11], and W. W. Zhu[16]

[1] Dept. of Physics and McGill Space Institute, McGill University, Montreal, QC H3A 2T8, Canada
[2] NRAO, 520 Edgemont Road, Charlottesville, VA 22903, USA
[3] Max-Planck-Institut für Radioastronomie, Auf dem Hügel 69, Bonn D-53121, Germany
[4] Cornell Center for Astrophysics and Planetary Science, Ithaca, NY 14853, USA
[5] South African Radio Astronomy Observatory, Observatory, 7925, South Africa
[6] Department of Physics and Astronomy, Franklin and Marshall College, Lancaster, PA 17604-3003, USA
[7] George Mason University, resident at the Naval Research Laboratory, Washington, DC 20375, USA
[8] School of Chemistry, University of East Anglia, Norwich Research Park, Norwich NR4 7TJ, UK
[9] ASTRON, the Netherlands Institute for Radio Astronomy, Oude Hoogeveensedijk 4, 7991 PD Dwingeloo, The Netherlands
[10] Anton Pannekoek Institute for Astronomy, University of Amsterdam, Postbus 94249, 1090 GE Amsterdam, The Netherlands
[11] JBCA, School of Physics & Astronomy, University of Manchester, Manchester, M13 9PL, UK
[12] Department of Physics and Astronomy, West Virginia University, Morgantown, WV 26501, USA
[13] Center for Gravitational Waves and Cosmology, West Virginia University, Chestnut Ridge Research Building, Morgantown, WV 26505, USA
[14] Dominion Radio Astrophysical Observatory, Herzberg Astronomy & Astrophysics Research Centre, National Reseach Council Canada, P.O. Box 248, Penticton, V2A 6J9, Canada
[15] Department of Physics and Astronomy, University of British Columbia, 6224 Agricultural Road, Vancouver, BC V6T 1Z1 Canada
[16] CAS Key Laboratory of FAST, NAOC, Chinese Academy of Sciences, Beijing 100101, People's Republic of China

Abstract

We report on eight millisecond pulsars (MSPs) in binary systems discovered with the Arecibo L-Band Feed Array (PALFA) pulsar survey. Phase-coherent timing solutions derived from 2.5–5 yr of observations carried out at the Arecibo and Jodrell Bank observatories are provided. PSR J1921+1929 is a 2.65 ms pulsar in a 39.6 day orbit for which we detect γ-ray pulsations in archival *Fermi* data. PSR J1928+1245 is a very low-mass-function system with an orbital period of 3.3 hr that belongs to the non-eclipsing black widow population. We also present PSR J1932+1756, the longest-orbital-period (41.5 days) intermediate-mass binary pulsar known to date. In light of the numerous discoveries of binary MSPs over the past years, we characterize the Galactic distribution of known MSP binaries in terms of binary class. Our results support and strengthen previous claims that the scatter in the Galactic scale height distribution correlates inversely with the binary mass function. We provide evidence of observational biases against detecting the most recycled pulsars near the Galactic plane, which overestimates the scale height of lighter systems. A possible bimodality in the mass function of MSPs with massive white dwarfs is also reported.

1. Introduction

Millisecond pulsars (MSPs) are short-period ($P \lesssim 100$ ms) neutron stars that differ from normal pulsars primarily because of their remarkably small spin-down rates ($\dot{P} \lesssim 10^{-17}$) and their different evolutionary histories. Only ~1% of all normal pulsars are in binary systems, while we observe orbiting companions (predominantly white dwarfs) in around 80% of MSPs. Their properties are consistent with them being old pulsars that have been spun up by the accretion of material from a companion (Alpar et al. 1982; Radhakrishnan & Srinivasan 1982; Bhattacharya & van den Heuvel 1991). For this reason, they are often referred to as "recycled pulsars." While the generally accepted definition of MSPs is pulsars having $P \lesssim 30$ ms, we shall apply throughout this work the broader definition proposed in Manchester (2017): pulsars with $P < 100$ ms whose $\dot{P}$ is smaller than 10^{-17}. This allows us to include many pulsars having had short-lived recycling phases (e.g., PSR J1753−2240) while excluding young pulsars (e.g., the Crab pulsar B0531+21). To date, more than 300 MSPs have been discovered, representing ~10% of the total known pulsar population,[17] and roughly half of those are found in globular clusters.[18]

The extraordinarily stable rotation of most MSPs allows us to use them as celestial clocks in a variety of applications. One notable example is their use as probes of binary motion, enabling precise neutron-star mass measurements and tests of relativistic gravitational theories. Such studies led to the first confirmation of the existence of gravitational radiation (Taylor et al. 1979) predicted by the theory of general relativity.

The continued discoveries of MSPs is also motivated by the effort to detect nanohertz gravitational waves (GWs) emitted by a cosmological population of supermassive black hole binaries via a "pulsar timing array" (PTA; Hellings & Downs 1983; Foster & Backer 1990; Jaffe & Backer 2003; Hobbs et al. 2010). This effort relies on the stability of the MSPs forming the array and the

---

[17] http://www.atnf.csiro.au/research/pulsar/psrcat/ (Manchester et al. 2005), version 1.60 of the ATNF Pulsar Catalogue.
[18] According to the Pulsars in Globular Clusters Catalogue available at http://www.naic.edu/~pfreire/GCpsr.html.

expected disturbances in the pulse times of arrival (TOAs) by passing GWs. Correlations in those disturbances as a function of angular separation are then inspected to identify potential signals in the form of a stochastic background. Improving PTA sensitivities is most effectively achieved by increasing the number of MSPs with high timing precision (Siemens et al. 2013). The GW signals detectable by PTAs are in the nanohertz frequency range, many orders of magnitude below the band where laser-interferometer systems, such as aLIGO (Abbott et al. 2009), are sensitive. PTA efforts are therefore complementary to interferometric ground-based detectors and can ultimately reveal information about the kinematics, morphology, content, and feedback mechanisms of galaxies.

The Arecibo L-Band Feed Array (PALFA) pulsar survey uses the 7-beam Arecibo *L*-band Feed Array (ALFA) on the Arecibo Observatory (AO) William E. Gordon 305 m telescope in Puerto Rico. It has been surveying low-latitude regions of the Galactic plane at 1.4 GHz since 2004 (Cordes et al. 2006; Lazarus et al. 2015). The great sensitivity of PALFA and its observational parameters (see Section 2) are excellent for finding faint, highly dispersed pulsars. To date, the survey has discovered 192 pulsars,[19] including three double neutron star (DNS) systems (Lorimer et al. 2006; van Leeuwen et al. 2015; Lazarus et al. 2016; Stovall et al. 2018) and 40 highly recycled MSPs[20] (e.g., Champion et al. 2008; Crawford et al. 2012; Deneva et al. 2012; Knispel et al. 2015; Scholz et al. 2015; Stovall et al. 2016) in the Galactic plane. Two PALFA discoveries, PSR J1903+0327 (Champion et al. 2008) and PSR J0557+1551 (Scholz et al. 2015), have been included in the NANOGrav PTA (Arzoumanian et al. 2018).

In this work, we present timing solutions for eight MSPs in binary systems recently discovered in the PALFA survey: PSRs J1906+0454, J1913+0618, J1921+1929, J1928+1245, J1930+2441, J1932+1756, J1937+1658, and J2010+3051. In Section 2, we describe the discovery and follow-up observations, as well as the timing analysis. The properties of individual pulsars are discussed in Section 3, and we examine the Galactic distribution of different MSP-binary classes in Section 4. Our results are summarized in Section 5.

2. Observations and Analysis

PALFA conducts a survey for pulsars and transients in the Galactic plane ($|b| < 5°$). The Mock spectrometers are used as a back end for the ALFA receiver, providing 322.6 MHz of bandwidth divided into 960 channels centered at 1375.5 MHz. The channels are sampled every 64 μs. PALFA surveys the two regions of the Galactic plane that lie in the region of the sky between a decl. of $0°–36°$ that can be observed with the telescope: the "inner" ($32° < l < 77°$) and "outer" ($168° < l < 214°$) Galaxy regions. The integration times for those longitude ranges are 268 and 180 s, respectively.

The survey data are processed by two independent pipelines. The first is a reduced-resolution "Quicklook" pipeline (Stovall 2013) performed in near real time onsite and which enables rapid discovery of bright pulsars. The second is a full-resolution PRESTO-based pipeline. It processes the data at a Compute Canada/Calcul Québec facility hosted at McGill

University and searches for pulsars in the Fourier domain. It also searches in the time domain, for pulsars with a fast-folding algorithm (Parent et al. 2018), and has a single-pulse pipeline (Patel et al. 2018) that searches for rotating radio transients and fast radio bursts. For a more detailed description of the survey, see Lazarus et al. (2015).

2.1. Discovery

The eight MSPs presented in this work were all discovered in the 268 sec inner-Galaxy pointings between 2014 June and 2016 November. Four of them (PSRs J1921+1929, J1930+2441, J1937+1658, and J2010+3051) were first identified by the "Quicklook" pipeline, while PSRs J1906+0454, J1913+0618, J1928+1245, and J1932+1756 were detected by the full-resolution pipeline only. Additional observations were then carried out to confirm the new sources.

2.2. Timing Observations

To determine the rotational, astrometric, and binary parameters of the systems, follow-up observations for all eight pulsars were conducted at AO using the dual-linear-feed *L*-wide receiver. In order to obtain timing solutions rapidly when pulsars were added to our timing program, three pulsars (PSRs J1930+2441, J1932+1756, and J2010+3051) had additional data taken with the Lovell Telescope at Jodrell Bank Observatory (JBO). The other sources were not observed at JBO as a result of the limited availability of the instrument at the time the pulsars were discovered.

Observations at AO have a nominal observing frequency range of 980–1780 MHz and an average system equivalent flux density of 2.9 Jy. However, frequencies at the edges of the band are removed and following RFI excision, only ~80% of the data is usable, resulting in an effective band of approximately 1050–1700 MHz. The Puerto Rico Ultimate Pulsar Processing Instrument (PUPPI) back end was used to record data. Depending on the discovery detection significance and the available time, we initially observed each pulsar for 300, 600, or 900 s per session in PUPPI's incoherent-dedispersion search mode. This mode provides total intensity data with 2048 channels readout every 40.96 μs. We then downsampled the data to 128 channels, correcting for dispersion delay due to plasma in the interstellar medium before summing channels. Data that were more affected by interference instead had frequency resolution reduced to 256 channels in order to optimize RFI mitigation. Once initial estimates of the ephemerides were obtained, the PUPPI observations were taken in coherent-dedispersion fold mode. In this mode, full-Stokes polarization data are folded at the predicted pulse period and recorded into 2048 profile bins in real time with 512 frequency channels. The data within each frequency channel are coherently dedispersed to a fiducial best-estimate value. Due to technical issues affecting the local oscillator at Arecibo starting in Summer 2018, some of the most recent data were taken in incoherent search mode.

Observations carried out with the 76 m Lovell Telescope at JBO used a dual-polarization cryogenic receiver having a system noise equivalent flux density on cold sky of 25 Jy. A passband from 1350–1700 MHz was processed using a digital filterbank that split the two polarization bands into 0.5 MHz wide channels. The power from each channel was then folded at the nominal topocentric period and the resultant profiles were dedispersed at the dispersion measure (DM) of the pulsar

---

[19] Pulsar discoveries are available on PALFA's discoveries page: http://www.naic.edu/~palfa/newpulsars/.
[20] Excluding those in this paper, seven PALFA-discovered MSPs have not yet been published, but discovery plots are available on PALFA's discoveries page.

and then summed. Each observation was typically of 30–60 minutes in duration.

2.3. Timing Analysis

Incoherent search mode data were cleaned of RFI, dedispersed into barycentric time series, and folded using `PRESTO` tools. From the search mode data taken during the first few months of follow-up observations, we obtained the best-fit period and period derivative of each barycentric fold and applied a model of orbital Doppler shifts with `PRESTO`'s `fitorbit` tool. The resulting binary parameters were used as starting points to produce ephemerides.

The coherently dedispersed data were calibrated, cleaned of RFI, and downsampled both in time and frequency, and pulse TOAs were extracted. Profile templates were initially created for each pulsar by fitting Gaussian components to the folded profile of the strongest detection. These standard templates were then used to extract TOAs with `PSRCHIVE`.

Initial phase-coherent ephemerides for five pulsars (PSRs J1906+0454, J1921+1929, J1928+1245, J1930+2441, and J1932+1756) were obtained using `Dracula`, a new algorithm for determining the correct global rotational count with a minimal number of `TEMPO` (a widely used program for analyzing pulsar timing data) iterations for pulsars with sparse timing data. This allowed us to eliminate ambiguity in the number of pulses between observations in the early stages of the phase connection process (i.e., data not sampled densely enough and/or not sampling the orbital phase well enough).

Improved, high-signal-to-noise standard templates were produced for each pulsar by summing frequency- and time-scrunched profiles from multiple observations conducted at AO. Signal-to-noise-based weightings were applied while summing the profiles. Profile baselines were set to zero and the final templates (shown in Figure 1) were smoothed using the `PSRCHIVE` tool `psrsmooth`, which applies a wavelet smoothing algorithm to create a noise-free template profile (Coifman & Donoho 1995; Demorest et al. 2013). We extracted high-precision TOAs by reducing further the frequency resolution to one to four channels and by folding the data down to one or two sub-integrations with `fold_psr-fits`, a component of the `psrfits_utils` library for processing PSRFITS pulsar data files. `PSRCHIVE`'s `pat` tool was used to extract TOAs by fitting for a linear phase gradient in the Fourier domain to determine the shifts between the profiles and the standard template (Taylor 1992). TOAs extracted from JBO data were obtained using a different profile template than those produced from Arecibo data. To account for this effect as well as other potential delays introduced by the use of different telescope back-end systems, we fitted for an arbitrary time offset between the two data sets.

Formal TOA uncertainties are often underestimated during the extraction procedures, and it is common practice in pulsar timing to increase their uncertainties by some scaling factor (`TEMPO`'s EFAC parameter) to produce a more conservative estimate of errors on the timing parameters. We list these factors in Table 1 along with the final `TEMPO` fits.

The DE421 solar system ephemeris and the UTC (NIST) terrestrial time standard were used in all timing solutions. Figure 2 shows our solution residuals.

Two binary orbital models were used throughout the analysis: the DD (Damour & Deruelle 1986) and ELL1 (Lange et al. 2001) models.

The DD model consists of an analytic solution for the equation of motion of binary pulsars using the first post-Newtonian approximation of general relativity. It is a theory-independent model that considers effects such as Shapiro delay and aberration due to the pulsar motion. This binary model was applied to two of the eight MSPs presented in this work (PSRs J1913+0618 and J1932+1756), but our current timing precision is insufficient to allow us to measure any post-Newtonian parameters.

The ELL1 timing model is a modification of the model above, adapted for small-eccentricity binary pulsars where the longitude of periastron, ω, and the time of periastron, T_0, are highly correlated. The ELL1 model avoids the covariance between ω and T_0 by parameterizing the orbit with the time of ascending node $T_{\rm asc} = T_0 - \omega P_b/2\pi$ and the first and second Laplace parameters, $\epsilon_1 = e \sin\omega$ and $\epsilon_2 = e \cos\omega$, where e is the eccentricity. This model accounts only for first-order corrections in e. It therefore applies to nearly circular orbits where $x\ e^2$ is much smaller than the error in TOA measurements, where x is the projected semimajor axis. The timing solutions of the six remaining MSPs were obtained using this model.

2.4. Polarization and Flux Density Measurements

Polarization calibrations were performed using observations of a noise diode before observing the pulsars in coherent mode with AO's L-wide receiver. For flux calibrations, we used NANOGrav observations of the bright quasars J1413+1509 and J1445+099 (The NANOGrav Collaboration et al. 2015). The same set of flux-calibrator data was used for all sources, therefore flux measurements are subjected to systematic errors in addition to statistical errors. Given the nature of our flux calibration technique, we believe that relative error estimates on the order of 20% are applicable. Both calibrations were conducted with `PSRCHIVE`'s tool `pac` using the *SingleAxis* model, assuming that the polarization of the two receptors are perfectly orthogonal. Polarization profiles for the eight pulsars are shown in Figure 3.

Following data calibration and RFI excision, we combined the data to increase the total linearly polarized flux and searched for rotation measures (RMs) ranging from -1000 to $1000\,{\rm rad\,m^{-2}}$ using `PSRCHIVE`'s `rmfit` tool. Due to the low brightness of the pulsars and the limited number of observations taken in fold mode that could be combined, we could only detect an RM at a significant level for three sources (PSRs J1921+1929, J1928+1245, and J2010+3051). RM and average flux measurements are reported in Table 1.

Despite showing significant linearly polarized flux and position angle detections for multiple profile bins, the RM value determined from our current data set for PSR J1937+1658 is consistent with being zero (see Figure 3).

Using polarization information of NANOGrav pulsar data taken at AO, Gentile et al. (2018) demonstrated that there is an asymmetry in the line-of-sight component of the Galactic magnetic field about a Galactic latitude of $0°$, producing RM values near zero for the lowest-latitude sources (see Figure 20 in Gentile et al. 2018). It is therefore likely that PSR J1937+1658 is located in an environment where the Galactic magnetic field has a small component toward our line of sight, resulting in an RM close to zero.

We note a flux enhancement for PSR J1937+1658 during 2015 November, before which the flux was fairly stable around
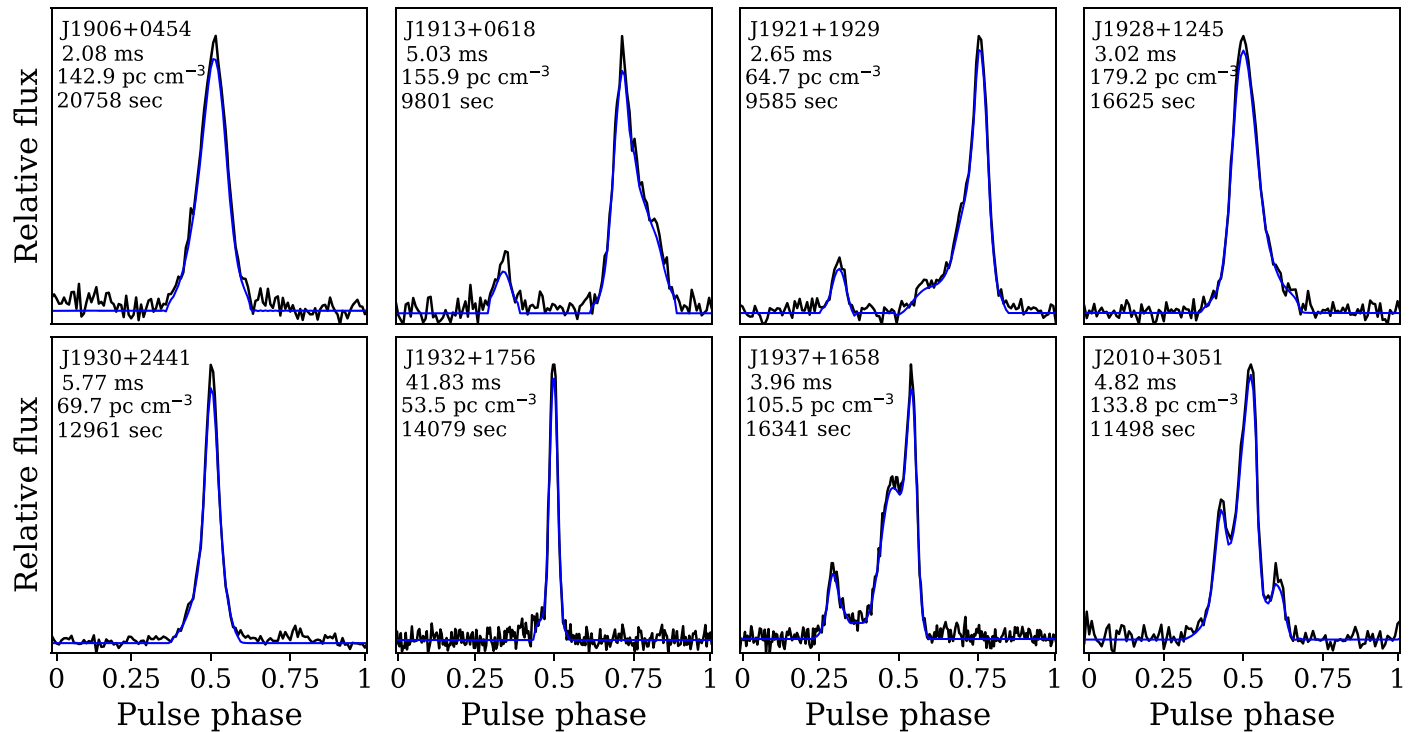
Figure 1. High-signal-to-noise pulse profiles at 1.4 GHz of the eight pulsars presented in this work. Black curves correspond to the phase-aligned and summed observations, and the blue curves are the smoothed standard templates used to generate TOAs. One full period is shown in either 128 or 256 phase bins. The name, rotation period, DM, and the total integration time used to generate the profiles are indicated for each pulsar in their respective profile subplot. Smoothed templates are provided on Zenodo (doi:10.5281/zenodo.3515416).

45 μJy (see Figure 4). It then reached $\sim$200 μJy by the end of the month, and the flux subsequently remained at $\sim$140 μJy.

If we assume the pulsar's luminosity to be approximately constant, refractive interstellar scintillation (RISS) resulting from focusing and defocusing of light by large scale (10^{11}–10^{13} cm) electron density inhomogeneities could explain this variation in flux density (Sieber 1982; Rickett et al. 1984). While diffractive scintillation by smaller-scale inhomogeneities can cause variations in compact radio sources on minutes to hours timescales (Scheuer 1968; Cordes et al. 1985), RISS produces slower (days to weeks) variations (e.g., Stinebring & Condon 1990).

Higher-cadence, dedicated observations having longer integrations and more rigorous flux calibration (where the calibrator data are taken during the same session) would be needed to properly characterize the various contributions of propagation effects to this flux variation.

3. Properties of New Discoveries

All pulsars presented in this paper were found at Galactic longitudes between 39° and 68°, and within 3° of the Galactic plane. Except for PSR J1932+1756 ($P = 41.8$ ms), they all have rotation periods shorter than 6 ms, adding to the low-B field population occupying the lower-left corner of the P–$\dot{P}$ diagram (see Figure 5). Their DM values range from 53–179 pc cm^{-3}, and five of them have DMs greater than 100 pc cm^{-3} (see Figure 6). Distances were estimated using both the NE2001 Galactic density electron model (Cordes & Lazio 2002) and the (Yao et al. 2017, hereafter YMW16) model. The distances estimated with the two models agreed with each other well within the estimated 25% uncertainty for

all pulsars. Throughout the rest of this work, we will refer to distance predictions from the YMW16 model to be consistent with the ATNF Pulsar Catalogue, which applied that model to all database entries relying on distance estimates (as of 2016 November).

Measured and derived pulsar parameters are reported in Table 1, and some of their most notable properties are discussed below. We first present the derivations of intrinsic spin-down rates and upper limits on proper motions and distances.

3.1. Intrinsic Period Derivative Calculations

Aside from the intrinsic spin-down rate $\dot{P}_{\rm int}$ of the pulsar, there are several effects contributing to the observed period derivative, $\dot{P}_{\rm obs}$, and those can be significant for MSPs given their small $\dot{P}_{\rm int}$. In most cases, the kinematic effects contribute the most to the deviation of the $\dot{P}_{\rm obs}$ from $\dot{P}_{\rm int}$. Apparent accelerations arise as a result of transverse motions (Shklovskii effect; Shklovskii 1970) and relative accelerations between the pulsar and the solar system Barycenter (Damour & Taylor 1991). Proper motion and distance measurements allow us to calculate the kinematic contributions to the observed period derivative $\dot{P}_{\rm obs}$, and therefore predict $\dot{P}_{\rm int}$:

$$\dot{P}_{\rm int} = \dot{P}_{\rm obs} - \dot{P}_{\rm gal} - \dot{P}_{\rm Shk}, \qquad (1)$$

where $\dot{P}_{\rm gal}$ includes both a vertical component of the Galactic acceleration of the pulsar and the line-of-sight acceleration due to Galactic differential rotation between the solar system and the pulsar. $\dot{P}_{\rm Shk}$ is the result of the Shklovskii effect, and is

Table 1
Timing Parameters of PALFA-discovered MSPs

	J1906+0454	J1913+0618	J1921+1929	J1928+1245
R.A. (J2000)	19:06:47.13970(7)	19:13:17.8786(2)	19:21:23.35070(4)	19:28:45.39360(6)
Decl. (J2000)	+04:54:09.042(2)	+06:18:08.277(5)	+19:29:22.299(1)	+12:45:53.374(3)
Proper motion in R.A. (mas yr^{-1})	−6(1)	−9(2)	−3.2(8)	<3
Proper motion in decl. (mas yr^{-1})	−14(3)	<12	−11(1)	<15
Total proper motion, μ_T (mas yr^{-1})	15(3)	9(2)	12(1)	<15
Parallax, π (mas)	<12	<17	<9	<16
Spin frequency, ν (s^{-1})	480.01267196822(5)	198.93129209203(3)	377.88018632311(2)	330.94979452682(6)
Spin frequency derivative, $\dot{\nu}_{\rm obs}$ (10^{-15} s^{-2})	−0.687(3)	−0.3804(8)	−5.4542(7)	−1.84(1)
DM (pc cm^{-3})	142.793(2)	155.987(3)	64.7632(9)	179.233(1)
Orbital period, P_b (days)	7.04187028(1)	67.7439374(2)	39.64926375(2)	0.1366347269(8)
Projected semimajor axis, $x = a\sin i/c$ (lt-s)	4.350215(2)	32.742919(2)	20.8474224(7)	0.018951(1)
Time of periastron, T_0 (MJD)	⋯	57721.746(3)	⋯	⋯
Time of ascending node, $T_{\rm asc}$ (MJD)	58101.4031477(5)	⋯	57602.9409583(2)	57949.020215(3)
Eccentricity, e (10^{-4})	⋯	7.053(1)	⋯	⋯
1st Laplace parameter, $\epsilon_1 = e \sin \omega$ (10^{-4})	<0.03	⋯	0.8093(5)	<5
2nd Laplace parameter, $\epsilon_2 = e \cos \omega$ (10^{-4})	<0.02	⋯	−1.9182(6)	<4
Longitude of periastron, ω (deg)	⋯	38.65(2)	⋯	⋯
Galactic longitude, l (deg)	39.045	41.034	53.619	48.534
Galactic latitude, b (deg)	−1.167	−1.960	2.453	−2.290
Period, P (ms)	2.0832783349232(2)	5.0268612317532(8)	2.6463414494692(1)	3.0216063479651(5)
Period derivative, $\dot{P}_{\rm obs}$[a] (10^{-20})	0.298(1)	0.961(2)	3.8196(5)	0.168(1)
Mass function (10$^{-3} M_\odot$)	1.782539(2)	8.212853(2)	6.1882748(6)	0.0003914(1)
Minimum companion mass ($M_\odot$)	0.163	0.286	0.257	0.009
Median companion mass ($M_\odot$)	0.191	0.337	0.302	0.011
Surface dipolar magnetic field, B[b] (10^8 G)	0.8	1.8	3.2	0.7
Spin-down luminosity, $\dot{E}$[b] (10^{33} erg s^{-1})	13	2.0	81	2.4
Characteristic age, τ_c[b] (Gyr)	11	12	1.1	28
DM distance, D[c] (kpc)	4.1	5.9	2.4	6.1
Pulse width, W50[d] (ms)	0.20	0.47	0.17	0.28
Rotation measure, RM (rad m^{-2})	⋯	⋯	121(22)	60(17)
Mean flux density, S_{1400}[e] (mJy)	0.043(16)	0.06(1)	0.12(2)	0.08(2)
Mean luminosity, L_{1400}[f] (mJy kpc^2)	9	26	9	37
Follow-up site	AO	AO	AO	AO
Discovery observation date (MJD)	57258	56817	57573	57268
Reference epoch (MJD)	58100.0	57696.0	58137.0	57974.0
First TOA (MJD)	57520.34	56935.93	57595.19	57268.02
Last TOA (MJD)	58680.17	58456.78	58680.22	58680.21
Number of TOAs	143	131	123	135
Binary model	ELL1	DD	ELL1	ELL1
EFAC[g]	1.1	1.2	1	1
rms post-fit residuals (μs)	12.09	19.78	4.43	10.35
Daily-averaged rms post-fit residuals (μs)	8.42	6.06	2.40	2.63
Reduced χ^2	1.03	1.01	1.03	1.07

	J1930+2441	J1932+1756	J1937+1658	J2010+3051
R.A. (J2000)	19:30:45.39844(6)	19:32:07.2277(5)	19:37:24.90851(8)	20:10:03.9542(1)
Decl. (J2000)	+24:41:01.564(1)	+17:56:17.31(1)	+16:58:42.553(2)	+30:51:18.892(1)
Proper motion in R.A. (mas yr^{-1})	<4	−13(5)	−1.8(7)	−10.3(9)
Proper motion in decl. (mas yr^{-1})	−10(3)	<32	−5(1)	−3(1)
Total proper motion, μ_T (mas yr^{-1})	11(3)	15(7)	5(1)	10.8(9)
Parallax, π (mas)	16(6)	<66	<10	<19
Spin frequency, ν (s^{-1})	173.38814681699(2)	23.90555115685(1)	252.67407210877(1)	207.62936108328(2)
Spin frequency derivative, $\dot{\nu}_{\rm obs}$ (10^{-15} s^{-2})	−0.260(2)	−0.2470(3)	−0.8429(3)	−0.2098(7)
DM (pc cm^{-3})	69.572(1)	53.183(9)	105.840(1)	133.756(2)
Orbital period, P_b (days)	76.4059750(2)	41.5079763(1)	17.30610529(2)	23.35889575(2)
Projected semimajor axis, $x = a\sin i/c$ (lt-s)	29.748786(2)	68.85890(3)	9.2582711(9)	12.051767(1)
Time of periastron, T_0 (MJD)	⋯	57506.691(7)	⋯	⋯
Time of ascending node, $T_{\rm asc}$ (MJD)	58162.4048255(7)	⋯	57750.5735047(9)	57844.9713383(5)
Eccentricity, e (10^{-4})	⋯	2.468(4)	⋯	⋯
1st Laplace parameter, $\epsilon_1 = e \sin \omega$ (10^{-4})	1.210(1)	⋯	−0.374(2)	−0.056(2)
2nd Laplace parameter, $\epsilon_2 = e \cos \omega$ (10^{-4})	1.2920(9)	⋯	0.838(2)	−0.142(2)
Longitude of periastron, ω (deg)	⋯	−55.50(6)	⋯	⋯

Table 1
(Continued)

	J1906+0454	J1913+0618	J1921+1929	J1928+1245
Galactic longitude, l (deg)	59.228	53.464	53.237	68.967
Galactic latitude, b (deg)	3.002	−0.520	−2.090	−1.326
Period, P (ms)	5.7674069326981(6)	41.83128819908(2)	3.9576676453354(2)	4.8162745133088(4)
Period derivative, $\dot{P}_{obs}$[a] (10^{-20})	0.866(6)	43.22(5)	1.3203(4)	0.487(2)
Mass function ($10^{-3} M_\odot$)	4.8421235(8)	203.4697(2)	2.8449441(8)	3.444533(1)
Minimum companion mass ($M_\odot$)	0.235	1.077	0.193	0.207
Median companion mass ($M_\odot$)	0.276	1.325	0.226	0.243
Surface dipolar magnetic field, B[b] (10^8 G)	1.8	40	2.3	0.8
Spin-down luminosity, $\dot{E}$[b] (10^{33} erg s^{-1})	1.2	2.0	8.5	0.4
Characteristic age, τ_c[b] (Gyr)	16	1.8	4.7	66
DM distance, D[c] (kpc)	3.3	2.1	3.3	6.5
Pulse width, W50[d] (ms)	0.32	1.31	0.40	0.23
Rotation measure, RM (rad m^{-2})	…	…	…	-64(15)
Mean flux density, S_{1400}[e] (mJy)	0.08(2)	0.045(9)	0.09(2)	0.10(2)
Mean luminosity, L_{1400}[f] (mJy kpc^2)	11	2	12	53
Follow-up site	AO+JBO	AO+JBO	AO	AO+JBO
Discovery observation date (MJD)	57701	56537	56816	57209
Reference epoch (MJD)	58177.0	57516.0	57516.0	57949.0
First TOA (MJD)	57701.88	56537.03	56816.27	57218.800
Last TOA (MJD)	58653.28	58496.67	58653.25	58680.24
Number of TOAs	162	216	153	225
Binary model	ELL1	DD	ELL1	ELL1
EFAC[g]	1	1	1	1.25
rms post-fit residuals (μs)	8.88	51.92	6.88	13.31
Daily-averaged rms post-fit residuals (μs)	12.03	22.09	1.74	7.09
Reduced χ^2	0.74	1.04	1.07	1.00

Notes. Numbers in parentheses are TEMPO-reported uncertainties in the last digit quoted. The DE421 solar system ephemeris and the UTC (NIST) terrestrial time standard were used for all solutions. TEMPO-readable ephemeris files as well as the template profiles shown in Figure 1 are provided on Zenodo (doi:10.5281/zenodo. 3515416).
[a] Observed period derivative obtained from the timing analysis.
[b] Calculated using the derived intrinsic period derivative.
[c] DM-derived distance using the YMW16 Galactic electron density model.
[d] Pulse width at 50% of the peak at 1400 MHz (calculated on the primary peak when multiple components are present in the profile).
[e] Calculated at 1400 MHz.
[f] Daily-averaged and weighted rms residuals.
[g] Scaling factor used to increase TOA uncertainties.

calculated using the following equation (Shklovskii 1970):

$$\dot{P}_{Shk} = \frac{P}{c}\mu_T^2 D. \quad (2)$$

The terms P, μ_T, and D are the rotation period, the composite proper motion, and the distance, respectively.

When using μ_T directly from the timing analysis and the DM distances to calculate $\dot{P}_{int}$, we obtain a negative value for one of the pulsars. Using $\dot{P}_{obs}$ as an upper limit for the kinematic terms ($\dot{P}_{gal} + \dot{P}_{Shk}$), we can better estimate the uncertainty on our measurements and determine the most likely distance and proper motion for each pulsar.

Similarly to the technique performed by Ng et al. (2014), the contribution from each term in Equation (1) and their associated uncertainties were estimated via a Monte Carlo (MC) rejection sampling. For each pulsar, we generated sampling combinations of $\dot{P}_{obs}$, μ_T and D, each drawn from probability density functions of normal distributions having means equal to the measured values. Uncertainties of 25% were used to construct the distance distributions. For MSPs where we did not detect significant proper motions, we used the

measured upper limits as constraints. Calculated values for $\mu_{T,MC}$, D, and v_T are presented in Table 2. $\dot{P}_{gal}$, $\dot{P}_{shk}$, and $\dot{P}_{int}$ were computed for each combination, where we used the approximation from Lazaridis et al. (2009) (valid for Galactic height <1.5 kpc) for the vertical component contribution to the Galactic acceleration, and Equation (5) of Nice & Taylor (1995) for the line-of-sight relative acceleration. Values used for the Galactocentric distance of the solar system and the rotational speed of the Galaxy at the solar system are those derived in Reid et al. (2014).

In the rejection process, we assumed that MSPs are not gaining rotational energy (i.e., $\dot{P}_{int} > 0$) and that no additional gravitational potential significantly affects the observed period derivatives. Sampling combinations producing $D \leqslant 0$ or $\mu_T < 0$ were also rejected. The resulting mean values and their associated errors of the various estimations of the period derivatives (see Table 3) were calculated from 10^6 valid combinations of our MC iterations. We note that since estimations of Shklovskii accelerations correlate strongly with the measured μ_T and that most of our timing measurements only weakly constrain this parameter, the low-significance $\dot{P}_{Shk}$ values
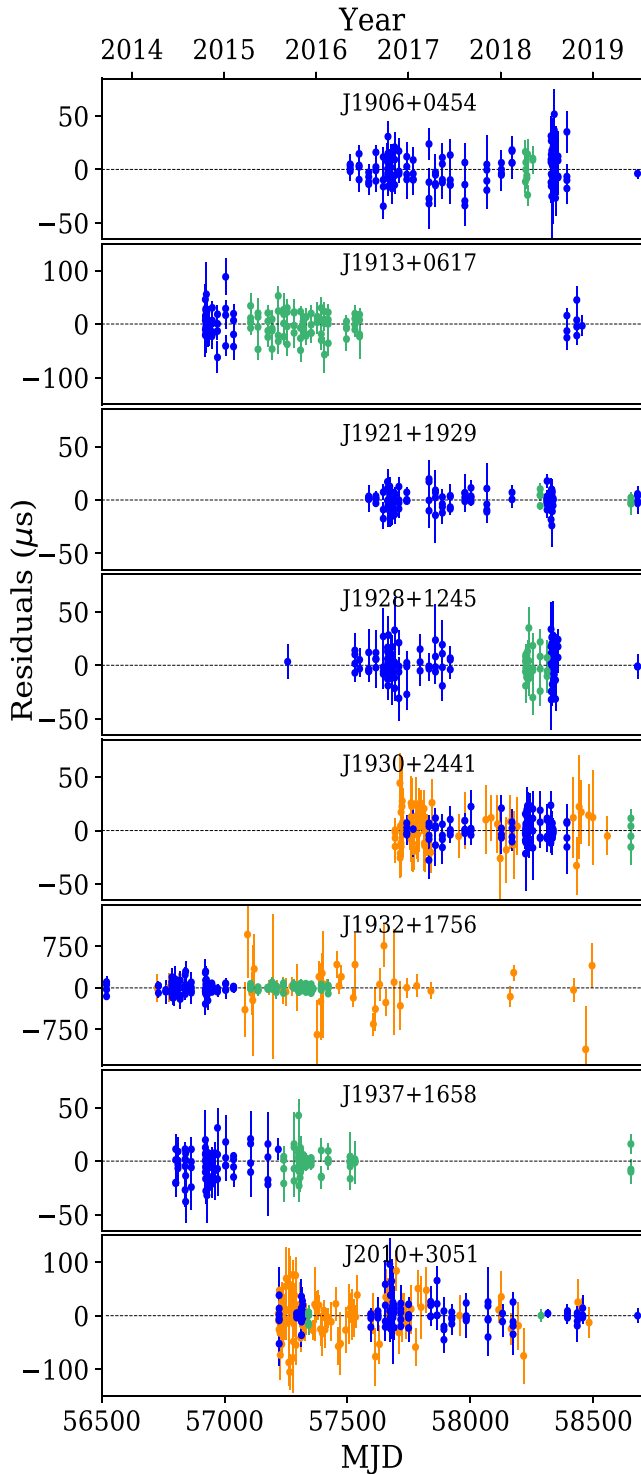
Figure 2. Timing residuals of the best-fit solutions for the eight MSPs presented in this work. The blue and green data points represent observations conducted at AO in search and fold mode, respectively, and the orange points are those obtained with the Lovell Telescope at JBO. When satisfactory timing solutions are obtained, pulsars are typically removed from our time-limited PALFA's regular timing program to allow the follow-up of other PALFA discoveries. Some pulsars (e.g., PSR J1937+1658) were re-observed after months of being excluded from the timing program in order to increase our precision on astrometric parameter measurements (such as the pulsar's proper motion).

relative errors are reduced by ∼20%. All distance estimates produced by our MC simulations are consistent with the values predicted by both the NE2001 and YMW16 models with average relative errors between 25% and 30%.

3.2. Timing Results

3.2.1. PSR J1906+0454

With a rotation period of 2.08 ms, PSR J1906+0454 is the most rapidly rotating MSP of the eight, and it is the second most rapidly rotating object found by the PALFA survey. The pulse width at half maximum (W50) is 0.20 ms, corresponding to a pulse duty cycle of 10%. According to the YMW16 model, its DM of 142.8 pc cm^{-3} predicts a distance of 4.1 kpc.

It is in a nearly circular 7.04 day orbit, the second shortest orbital period of the pulsars presented here. Assuming a pulsar mass M_p of 1.40 $M_\odot$ and an orbital inclination angle i of 60°, the median mass of the companion is 0.191 $M_\odot$. The proximity of PSR J1906+0454 to the companion mass-orbital period relation predicted by Tauris & Savonije (1999) for MSP–WD systems born from low-mass X-ray binaries (LMXBs) suggests that the companion is a low-mass helium white dwarf (He WD, see Figure 7). This hypothesis is further supported by the rapid rotation of the pulsar, indicating a past long-term accretion phase.

A total proper motion detection μ_T of 15 ± 3 mas yr^{-1} was obtained from the timing analysis, corresponding to a transverse velocity of 300 ± 90 km s^{-1} for a 4.1 kpc distance. Our MC simulations suggest a somewhat lower value of 199^{+45}_{-38} km s^{-1}.

After correcting for apparent accelerations arising from the Shklovskii effect and the Galactic potential, our calculations of the intrinsic period derivative give $\dot{P}_{int} = 0.07^{+0.04}_{-0.02} \times 10^{-20}$. The Shklovski effect is the most significant and accounts for nearly 85% of the observed spin-down.

Our timing solution spans 3.2 yr and has a post-fit rms timing residual of 12.09 μs.

3.2.2. PSR J1913+0618

PSR J1913+0618 has a spin period of 5.03 ms, an observed spin period derivative of 9.61×10^{-21} and a DM of 155.99 pc cm^{-3}. The DM-implied distance is 5.9 kpc. A 9.4% duty cycle main pulse with a weak interpulse are observed for this pulsar.

The orbital period of this system is 67.7 days and it has an eccentricity of 7×10^{-4}. Excluding DNSs, PSR J1913+0618 belongs to the top 15% most eccentric recycled pulsars in the Galactic field. The median companion mass is 0.34 $M_\odot$. According to the classification proposed by Tauris et al. (2012) and the position of this pulsar in both the orbital period-eccentricity and companion mass-orbital period diagrams (Figure 7), the nature of the companion is consistent with being either a massive He WD or a low-mass carbon–oxygen (CO) or oxygen–neon–magnesium (ONeMg) WD.

We measured $\mu_T = 9 \pm 2$ mas yr^{-1}, and the large distance of the pulsar implies a large transverse velocity of 250 ± 83 km s^{-1}, making PSR J1913+0618 among the top 10 highest transverse-velocity MSPs known in the Galactic plane.[21] The MC sampling suggests similar values (see Table 2).

Our timing solution spans 4.2 yr and has an rms residuals of 19.78 μs.

we report are expected. The most likely values produced by the simulations for the proper motions, $\mu_{T,MC}$, are all consistent with the measured μ_T values produced by the timing analysis, and the

---

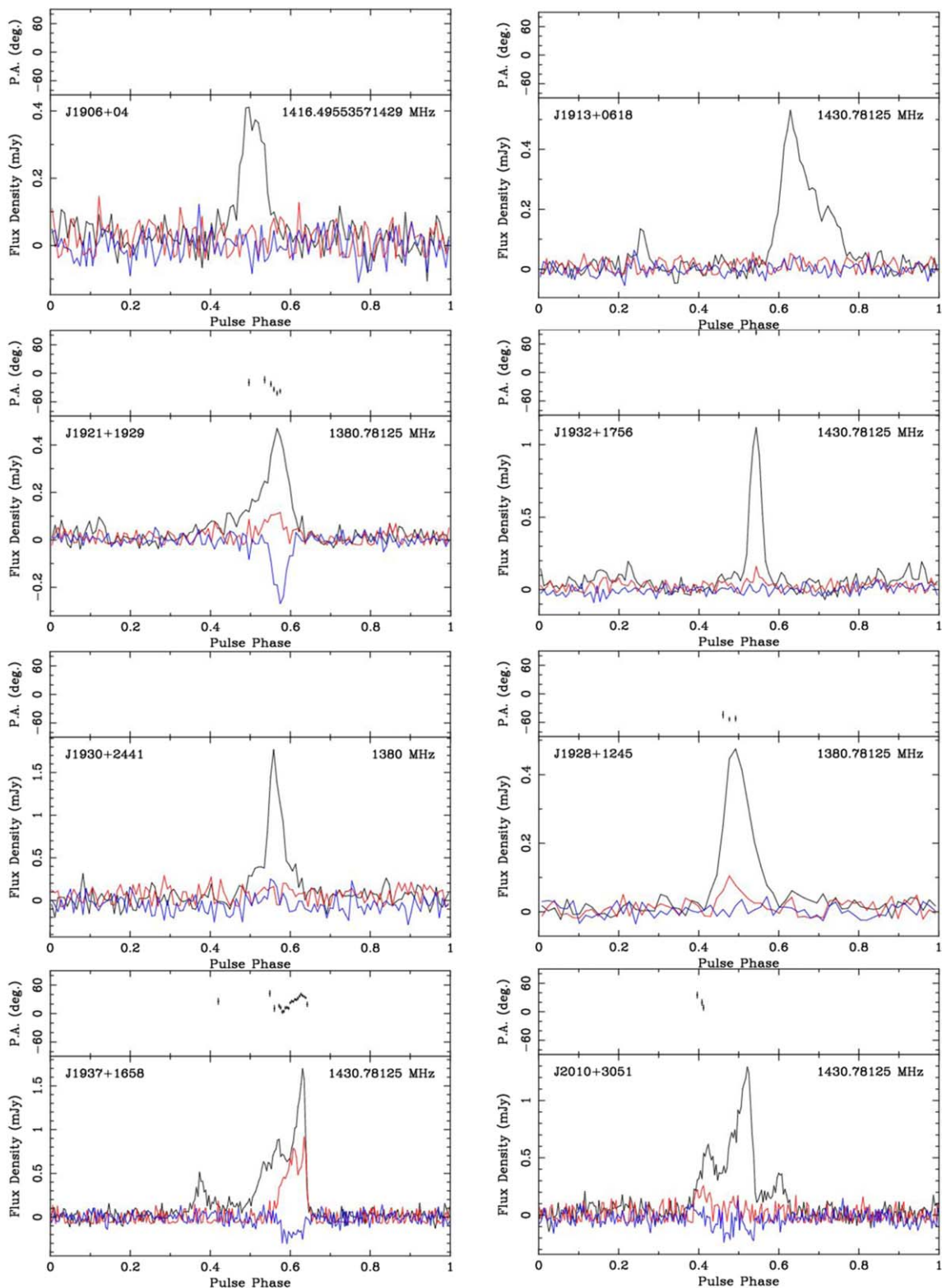[21] According to the ATNF Catalogue, version 1.60.

Figure 3. Polarization profiles for the eight MSPs presented in this work. Total (black), linearly polarized (red). and circularly polarized (blue) flux densities are shown in the bottom panel of each plot. The position angle of linear polarization for profile bins with a linear polarization greater than a signal-to-noise ratio of three are displayed in the panel above each profile plot. RM measurements could only be determined marginally for PSRs J1921+1929, J1928+1245, and J2010+3051 (see Table 1). Data for these three pulsars were corrected for Faraday rotation before folding. Only fully calibrated fold mode data have been folded to produce these profiles, representing only a small fraction of the full data set. Therefore, total flux density profiles do not have signal-to-noises as large as those in Figure 1. Note that while the profile PSR J1937+1658 shows significant linearly polarized flux, the RM determined from our current data set is consistent with being zero. Larger data sets will allow us to obtain more precise RM measurements.
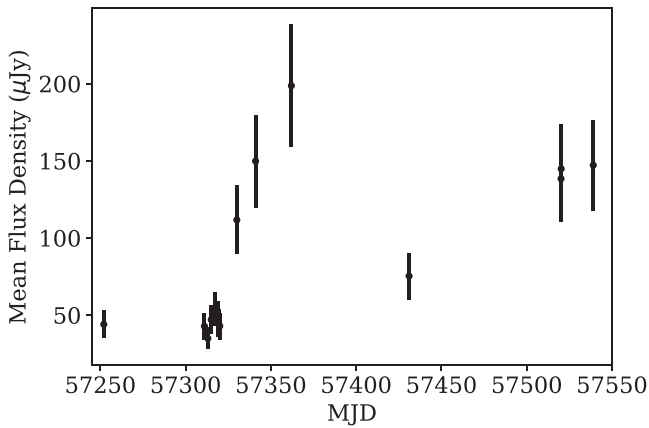
Figure 4. Variation in flux density measurements for PSR J1937+1658, calculated as described in Section 2.4.
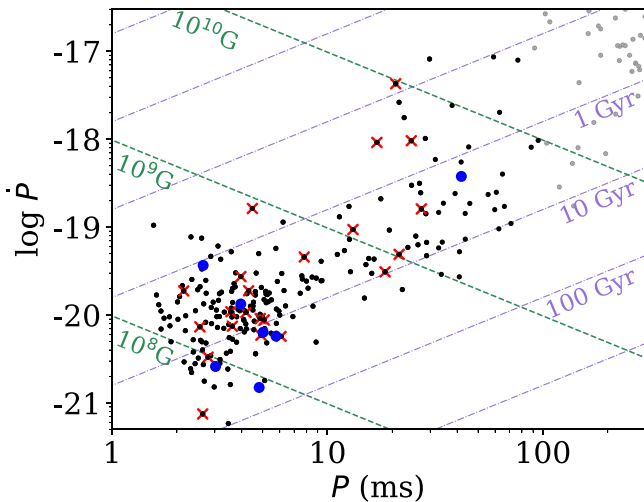
Figure 5. Period–period derivative (P–$\dot{P}$) diagram for pulsars with $P < 300$ ms. Black dots are MSPs ($P < 100$ ms and $\dot{P} < 1 \times 10^{-17}$), while the gray dots are normal (non-recycled) pulsars. Pulsars discovered by the PALFA survey are marked with red "X" symbols, and the eight MSPs presented in this paper are plotted with blue points. Green-dashed lines correspond to derived surface magnetic field strength at constant values of 10^8, 10^9, and 10^{10} G. Pulsar characteristic ages of 1, 10, and 100 Gyr are represented by purple-dashed lines. Data were taken from the ATNF Catalogue (version 1.60).

3.2.3. PSR J1921+1929

PSR J1921+1929 is a 2.45 ms pulsar with a DM of 64.8 pc cm^{-3} that is spatially coincident with a *Fermi* unassociated point source (Acero et al. 2015). We folded γ-ray photons with our timing solution and detected pulsations. Details on our analysis of the high-energy emission are presented in Section 3.3.

After correcting for the Shklovskii effect and accelerations in the Galactic potential, we obtain $\dot{P}_{int} = 3.65^{+0.03}_{-0.04} \times 10^{-20}$. This corresponds to a spin-down power $\dot{E}$ of 8.1×10^{34} erg s^{-1}, a typical value for radio-emitting γ-ray MSPs (see e.g., Abdo et al. 2013).

The binary system has an orbital period of 39.6 days and a median companion mass of 0.302 $M_\odot$, in very good agreement with the mass predicted by Tauris & Savonije (1999) for He WD companions. PSR J1921+1929 has orbital parameters that are consistent with being born from LMXBs, and combined with its short rotation period, the companion is most likely a He WD if we assume an inclination angle of 60°.
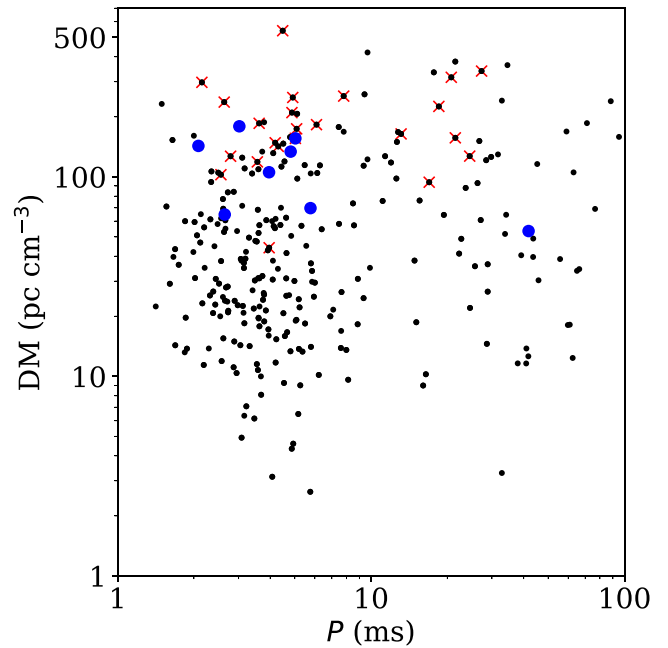
Figure 6. DM values of recycled pulsars (black dots) having measured $\dot{P}$, where the PALFA-discovered sources are marked with red "X" symbols. Blue points are the MSPs presented in this work. This figure illustrates the important contribution of the PALFA survey to the known population of high-DM MSPs, especially at short rotation periods.

The measured composite proper motion is 12 ± 1 mas yr^{-1}, but the current data do not allow us to measure a parallax distance (3σ upper limit of 9 mas).

We achieved a post-fit rms timing residual of 4.43 μs from 3 yr of data, the smallest residuals of the eight pulsars presented in this work. This source could be of possible interest for PTAs given its relatively low DM and rapid rotation.

3.2.4. PSR J1928+1245

PSR J1928+1245 has a spin period of 3.02 ms and the largest DM (179.2 pc cm^{-3}) of the eight MSPs presented in this paper, corresponding to a predicted distance of 6.1 kpc. It is one of the 10 most dispersed MSPs known. PSR J1928+1245 is in a short 3.28 hr orbit having a projected semimajor axis x of 0.019 lt-s. We also measure a first derivative of the orbital period, $\dot{P}_B$, at $34 \pm 5 \times 10^{-12}$. Based on those orbital parameters, the implied mass function (i.e., the lower limit on the mass of the unseen companion) is $3.9 \times 10^{-7} M_\odot$, one of the lowest among known MSPs. The minimum and median companion masses are 0.009 and 0.011 $M_\odot$, respectively. Those are properties commonly shared by "black widow" pulsars (Eichler & Levinson 1988; Fruchter et al. 1990): close binary systems in which the very low-mass companion (a nondegenerate or partially degenerate stellar core) is ablated by the pulsar wind. Black widows are typically found to have periods of a few milliseconds, in orbits with $P_b \lesssim 1$ day and have been suggested to be the progenitors of solitary MSPs. One can see by the position of PSR J1928+1245 in the left panel of Figure 7 (black-filled square in the lower-left corner) that it belongs to the black widow population. If the orbital inclination of such systems is high, plasma surrounding the companion may cause eclipses of the radio pulsar as it passes superior conjunction.
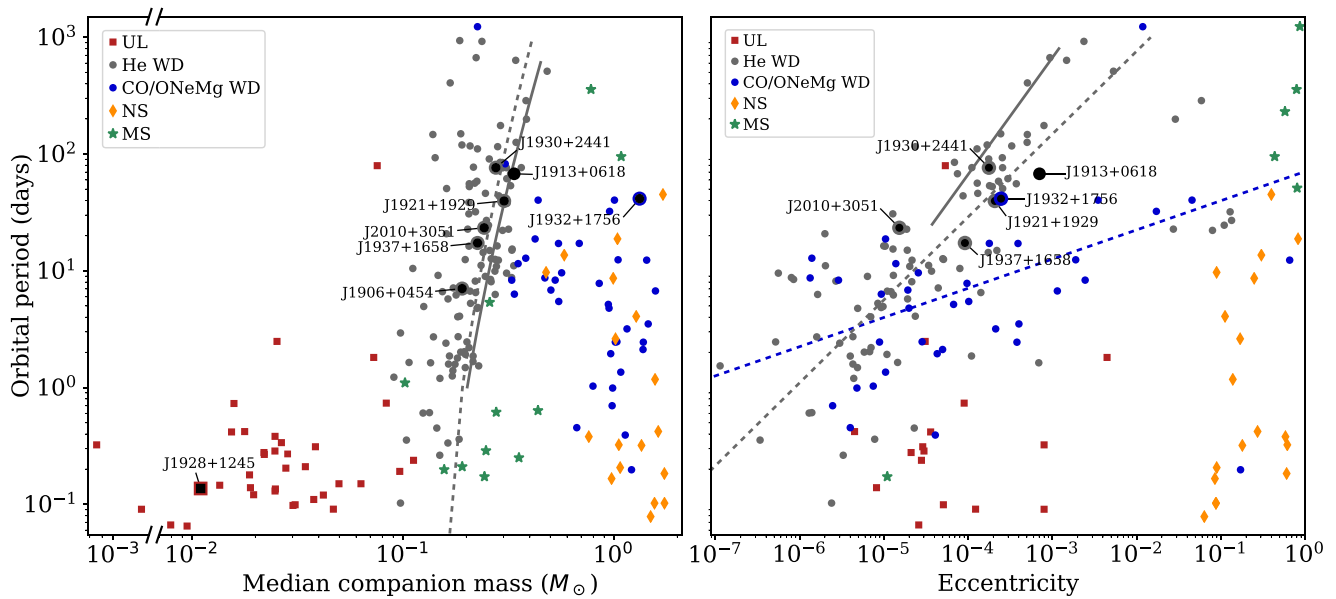
Figure 7. Orbital properties of Galactic MSPs in binary systems, taken from the ATNF Catalogue and the online Galactic MSP Catalog (http://astro.phys.wvu.edu/ GalacticMSPs/GalacticMSPs.txt). The different colors refer to the different companion types (see legend). UL refers to "ultra-light" companion, "NS" to neutron star, and "MS" to main-sequence star. MSPs presented in this work are labeled and represented by black-filled symbols. Left panel: orbital period as a function of derived median companion mass of stellar companions. The solid gray line is the theoretical prediction derived by Tauris & Savonije (1999) for MSP-He WDs systems formed from LMXBs, and the dashed line is the correlation found by Hui et al. (2018) for the same class. Right panel: eccentricity e vs. orbital period P_b for Galactic MSPs in binary systems. The prediction for the eccentricity of MSP-He WD systems with a given P_b derived in Phinney (1992), where the residual ellipticity is explained as a "freeze-out" during the companion transition from a red giant to a WD, is shown by the gray solid line. Gray and blue-dashed lines are the statistical correlations obtained by Hui et al. (2018) for the He and CO/ONeMg WD binary classes, respectively.

Table 2
Best-fit Values for the Total Proper Motion $\mu_{T,\mathrm{MC}}$, Distance D, Transverse Velocity v_T, and Corresponding 1σ Uncertainty Produced by the MC Method Described in Figure 5

PSR	$\mu_{T,\mathrm{MC}}$ (mas yr^{-1})	D (kpc)	v_T (km s^{-1})
J1906+0454	$12.4^{+1.4}_{-1.1}$	$3.4^{+0.7}_{-0.6}$	199^{+45}_{-38}
J1913+0618	$8.9^{+1.1}_{-1.2}$	$5.8^{+0.9}_{-0.9}$	245^{+47}_{-49}
J1921+1929	$11.5^{+0.6}_{-0.6}$	$2.4^{+0.4}_{-0.4}$	132^{+21}_{-21}
J1928+1245	$4.4^{+1.3}_{-1.3}$	$6.0^{+0.9}_{-0.9}$	126^{+42}_{-40}
J1930+2441	$9.7^{+1.5}_{-1.7}$	$3.2^{+0.5}_{-0.5}$	153^{+31}_{-34}
J1932+1756	$15.3^{+4.1}_{-3.7}$	$2.1^{+0.3}_{-0.3}$	153^{+47}_{-44}
J1937+1658	$5.0^{+0.6}_{-0.6}$	$3.3^{+0.5}_{-0.5}$	77^{+14}_{-14}
J2010+3051	$10.1^{+0.5}_{-0.5}$	$5.1^{+0.8}_{-0.8}$	244^{+38}_{-38}

Note. Initial uncertainties on the distance were set to 25%.

Table 3
Contributions to the Observed Period Derivatives $\dot{P}_{\mathrm{obs}}$

PSR	$\dot{P}_{\mathrm{obs}}$ (10^{-20})	$\dot{P}_{\mathrm{gal}}$ (10^{-20})	$\dot{P}_{\mathrm{Shk}}$ (10^{-20})	$\dot{P}_{\mathrm{int}}$ (10^{-20})
J1906+0454	0.298(1)	$-0.02^{+0.007}_{-0.02}$	$0.25^{+0.03}_{-0.04}$	$0.07^{+0.04}_{-0.04}$
J1913+0618	0.961(2)	$-0.3^{+0.07}_{-0.08}$	$0.58^{+0.19}_{-0.13}$	$0.64^{+0.13}_{-0.15}$
J1921+1929	3.8196(5)	$-0.04^{+0.008}_{-0.01}$	$0.21^{+0.04}_{-0.03}$	$3.65^{+0.03}_{-0.04}$
J1928+1245	0.168(3)	$-0.18^{+0.04}_{-0.03}$	$0.11^{+0.08}_{-0.03}$	$0.24^{+0.06}_{-0.07}$
J1930+2441	0.866(5)	$-0.16^{+0.03}_{-0.04}$	$0.45^{+0.16}_{-0.11}$	$0.58^{+0.11}_{-0.15}$
J1932+1756	43.22(5)	$-0.51^{+0.10}_{-0.14}$	$6.0^{+4.7}_{-1.7}$	$37.7^{+1.7}_{-4.6}$
J1937+1658	1.3203(4)	$-0.1^{+0.02}_{-0.03}$	$0.08^{+0.03}_{-0.02}$	$1.34^{+0.03}_{-0.02}$
J2010+3051	0.487(2)	$-0.23^{+0.04}_{-0.02}$	$0.60^{+0.05}_{-0.09}$	$0.12^{+0.06}_{-0.03}$

Note. Numbers in parentheses are 1σ uncertainties in the last digit quoted. Uncertainties on $\dot{P}_{\mathrm{Gal}}$, $\dot{P}_{\mathrm{Shk}}$, and $\dot{P}_{\mathrm{int}}$ are calculated using the MC method described in Figure 5.

Our observations that cover orbital phases corresponding to superior conjunction show no evidence for eclipsing or flux reduction. The non-detection of eclipses combined with a very low-mass function could imply that the system is far from edge-on, as is suggested by the apparent correlation between the orbital inclination and the presence of eclipses (Freire 2005; Ng et al. 2014; Guillemot et al. 2019).

Current data do not allow us to measure a proper motion for the pulsar, but the best-value $\mu_{T,\mathrm{MC}}$ we obtain is 4.4 ± 1.3 mas yr^{-1}.

Our solution spans 3.9 yr and has a post-fit rms residual of 10.35 μs.

3.2.5. PSR J1930+2441

PSR J1930+2441 is a 5.77-ms pulsar and has a DM of 69.6 pc cm^{-3}, implying a distance of 3.3 kpc. It is also the most

recent discovery (2016 November) we present in this work. The orbital period of this binary system is 76.4 days and the companion has a derived median mass of 0.28 $M_\odot$. The orbital parameters and the short spin period suggest that a He WD is the most likely companion type for this pulsar.

We measure a total proper motion μ_T of 10 ± 3 mas yr^{-1} and a parallax distance of 16 ± 7 mas. Values produced by our MC simulations are consistent with timing measurements and the estimated transverse velocity is 155 ± 60 km s^{-1}. However, given the short time span of the data set available for this pulsar, future proper motion measurements may vary from the quoted values given that they are highly covariant with other parameters.

Its timing solution has a post-fit rms residual of 8.88 μs and spans 2.6 yr.

3.2.6. PSR J1932+1756

PSR J1932+1756 has the longest rotation period of the eight MSPs with $P = 41.83$ ms. It has a DM of 53.2 pc cm^{-3} and an implied distance of 2.1 kpc.

The binary system has a 41.5 day period and for a 1.4 $M_\odot$ MSP, the companion must have a mass of at least 1.1 $M_\odot$ (median mass of 1.3 $M_\odot$). The low eccentricity ($e = 2.5 \times 10^{-4}$) of the orbit suggests that this massive companion is not a neutron star.

Subtracting the contribution of the Galactic acceleration and the Shklovskii effect to the observed $\dot{P}_{obs}$, we obtain a $\dot{P}_{int}$ of $\sim 3.8 \times 10^{-19}$ and infer a surface magnetic field B of 4×10^9 G. Those parameters indicate that the pulsar is old and has been recycled.

PSR J1932+1756 shares the characteristics of the inter-mediate-mass binary pulsar (IMBPs) class (Camilo et al. 2001), which have spin periods of a few tens of milliseconds, median companion masses $\geqslant 0.5 M_\odot$, and eccentricities larger than the low-mass binary pulsars. This pulsar has the longest orbital period of the known IMBPs. For systems with orbital periods longer than a few days, the most probable formation channel involves a short-lived phase of super-Eddington mass transfer on a timescale of a few Myr. During this process, the system also has to avoid a common-envelope phase (Tauris et al. 2000), otherwise frictional forces would result in the neutron star spiraling in and collapsing into a black hole. Heavy WDs having shallow convective envelopes can provide a formation channel for such systems when $P_B \sim 3$–50 days (Tauris et al. 2000).

We obtained a timing rms residual of 51.92 μs, spanning a 5.4 yr period. If the orbital inclination is favorable, PSR J1932+1756 could be a potential candidate for a future Shapiro delay measurement. However the rather large timing residual would make this measurement difficult. Our timing data currently do not allow us to detect any Shapiro delay.

3.2.7. PSR J1937+1658

PSR J1937+1658 has a spin period of 3.96 ms, a DM of 105.8 pc cm^{-3} implying a distance of 3.3 kpc, and has a complex pulse profile structure. It is a 17.3 day orbit with a derived eccentricity of $e = 9 \times 10^{-5}$ and a median companion mass of 0.23 $M_\odot$. A He WD is the most likely companion for this pulsar, as suggests its position on the orbital period-companion mass diagram in Figure 7.

We measure a small proper motion μ_T of 5 ± 1 mas yr^{-1}, corresponding to a small transverse velocity of 77 ± 24 km s^{-1}. Similar values are obtained from the MC rejection technique.

Our timing solution has an rms residual of 6.88 μs and spans 5 yr.

3.2.8. PSR J2010+3051

PSR J2010+3051 is a 4.8 ms pulsar with a DM of 133.8 pc cm^{-3} and is the most distant (DM-implied distance of 6.5 kpc) of the MSPs presented in this work. The orbital period of this nearly circular orbit binary is 23.4 days with a median companion mass of 0.243 $M_\odot$. This system shares orbital properties similar to those of PSR J1937+1658, and is located near that source on the period-companion mass diagram (Figure 7).

Our best-fit proper motion ($\mu_{T,MC} = 10.1 \pm 0.5$ mas yr^{-1}) and distance ($D = 5.1$ kpc) resulting from the MC sampling implies a large transverse velocity of 244 ± 38 km s^{-1}. Correcting for the kinematic contributions to $\dot{P}_{obs}$ results in $\dot{P}_{int} \sim 1.2 \times 10^{-21}$.

We achieve a post-fit rms residual of 13.31 μs for a solution spanning a 4 yr period.

3.3. Multiwavelength Counterparts

Archival optical and infrared data[22] were examined to identify possible counterparts to the eight MSPs. Point sources from either the Two Micron All-Sky Survey (Skrutskie et al. 2006) or the GAIA DR1 (Gaia Collaboration et al. 2017) catalogs that have positions consistent with being associated with PSRs J1913+0618, J1928+1245, and J1932+1756 were identified. However, even when adopting the 95% lower limit for the pulsar distances with minimal visual extinction and the companion being the hottest/most luminous WDs possible, all the possible infrared or optical counterparts have apparent magnitudes too bright to be consistent with being the true pulsar system counterpart. Considering the large distances of the pulsars presented here and their locations within crowded fields where the large amounts of dust and gas cause considerable optical extinction (total extinction, A_ν, between ~ 0.75 and 2.5 mag for the measured hydrogen column densities), finding associations to our systems is unlikely. Given that PSR J1932+1756 is the nearest source and has a relatively small characteristic age ($\tau_c \sim 1.5$ Gyr), it should be an interesting prospect for optical or infrared counterpart detection from future follow-up observations, however the WD companion is expected to have a mass larger than 1 $M_\odot$ and therefore should be small in size, making detection unlikely. Even by considering the most optimistic scenario for the WD properties and assuming little extinction, apparent magnitudes in near-infrared would still be $\gtrsim 25$.

We have inspected X-ray catalogs from the missions ASCA (Sugizaki et al. 2001), Chandra (CXOGSG, Wang et al. 2016), ROSAT (2RXS, Boller et al. 2016), RXTE,[23] Swift,[24] and XMM-Newton (XMMSL1, Saxton et al. 2008) for possible counterparts. No source with position within $2'$ from the MSP locations was found.

We also searched for high-energy counterparts using the Fermi Large Array Telescope (LAT) 4 yr Point Source Catalog[25] (Acero et al. 2015). The 4σ significance Fermi unassociated source 3FGL J1921.6+1934 has a position that coincides with PSR J1921+1929 (within the Fermi position error of $4'$). This source has a power-law-type spectrum and γ-ray spectral index of -2.5, properties that are typical for pulsars emitting high-energy photons. Using the DM-implied distance for this pulsar and the energy flux reported in the LAT catalog (11.7×10^{-12} erg cm^{-2} s^{-1} in the 0.1–100 GeV range), we calculate a γ-ray luminosity L_γ of 8×10^{33} erg s^{-1} at energies 0.1–100 GeV. The corresponding γ-ray efficiency $\eta = L_\gamma/\dot{E}$ is approximately 0.1, a typical value according to the second catalog of γ-ray pulsars (Abdo et al. 2013). We note however that this value depends on the predicted distance to the pulsar, which has large uncertainty.

All photons from MJDs 56,000–58,500 with reconstructed directions within $2°$ of the radio timing position of PSR J1921
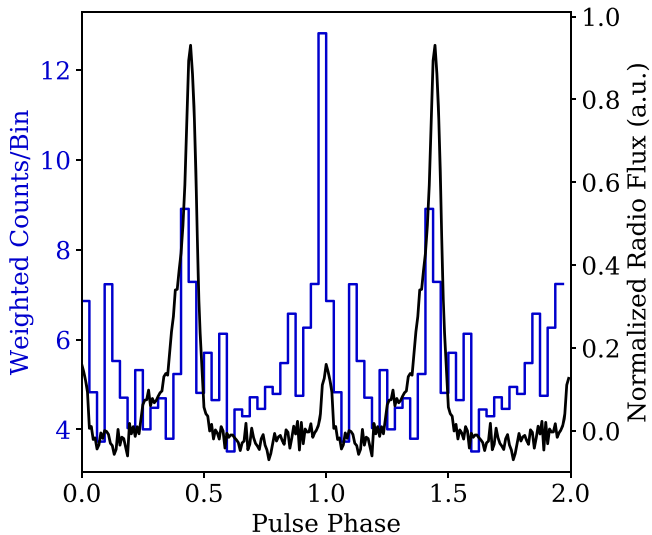

Figure 8. Radio (1.4 GHz; black curve) and γ-ray (0.1–300 GeV; blue curve) pulse profiles for PSR J1921+1929. For clarity, two full rotations are shown for the profiles. Phase alignment was obtained by folding photons using the same ephemeris, reference epoch, and template from the radio analysis.

+1929 that have energies in the 0.1–300 GeV range were retrieved, filtered, and barycentered using the event selection criteria recommended by the *Fermi* Science Support Center.[26] We rejected photons with weights smaller than 0.02 and phase-folded using the radio timing ephemeris presented in Table 1. The resulting detection has a H-test value (de Jager & Büsching 2010) of 129, corresponding to a 10σ significance. The phase-aligned radio and γ-ray pulse profiles are shown in Figure 8. Both profiles have aligned primary and a secondary peaks, but the primary/secondary γ-ray peak aligns with the secondary/primary radio peak.

The other pulsars reported in this work all have expected γ-ray flux $\sqrt{\bar{E}}/(4\pi D^2)$ (Abdo et al. 2013) below $8 \pm 3 \times 10^{14}$ erg s^{-1} kpc^{-2}. Furthermore, they are located within 3° from the Galactic plane where the high background of diffuse emission further makes detection difficult. Photons within 2° of the positions of the other pulsars were extracted, filtered, and phase-folded, but we did not detect any significant pulsations. Given the vast majority of known MSPs with estimated γ-ray flux $\sqrt{\bar{E}}/(4\pi D^2) < 10^{15}$ erg s^{-1} kpc^{-2} are not detected by *Fermi* (Smith et al. 2019), not detecting γ-ray pulsations for the remaining MSPs is expected.

In summary, we identify γ-ray pulsations for PSR J1921+1929, spatially coincident with the *Fermi* unassociated point-source 3FGL J1921.6+1934.

4. Discussion

Establishing a more complete census of the Galactic MSP population is key to understanding stellar and binary evolution in interacting systems. Currently, the known population is highly biased toward nearby sources ($D \lesssim 2$ kpc). Detecting distant MSPs allows us to better model the binary density distribution for different classes in terms of galactocentric radius and height. This not only contributes to expanding our knowledge of binary evolution, but can also help in designing surveys to target certain types of pulsars.

To date, 38 MSPs have been discovered by PALFA, including 29 that have been confirmed to be in binaries. Figure 6 shows that the DMs of PALFA-discovered MSPs are among the highest known, as already discussed by Crawford et al. (2012), Scholz et al. (2015), and Stovall et al. (2016). The average DM/P ratio is 13 pc cm^{-3} ms^{-1} for PALFA MSPs, three times larger than the non-PALFA recycled pulsars. Furthermore, they account for half of the known MSPs with DM > 150 pc cm^{-3}. Considering only the most recycled pulsars ($P < 10$ ms) at those DMs, 70% were discovered by PALFA and 11 of the 15 most dispersed were found by the survey. As a result of Arecibo's exceptional sensitivity and the high-resolution observations at *L*-band, our sensitivity to recycled pulsars is one of the highest, and matches the detectability limits predicted by the radiometer equation (Lazarus et al. 2015). Consequently, PALFA's contribution to unveiling the true MSP population in the Galactic field is among the most significant in radio pulsar surveys.

4.1. Spatial Distribution

When conducting population syntheses, a radial scaling is typically assumed when assigning the birth distribution of the population. Increasing the spatial extent covered by observed MSPs is therefore necessary to determine the best radial distribution to use as initial conditions.

Using both the YMW16 and NE2001 models, we map the Galactic distribution, projected onto the plane, of the observed population of radio MSPs in binaries. The results are shown in Figure 9, where ellipses represent the 2σ fits to the (X,Y) Galactic coordinates of the MSPs projected on the plane for the different binary classes. Looking at the location and distribution of points, one can see the observational bias toward nearby sources, especially for pulsars with UL and He WD companions judging by the smaller ellipses. Those pulsars have undergone longer accretion phases and thus have shorter spin periods than pulsars with massive CO/ONeMg WDs. Short-P pulsars are more difficult to find at larger distances in the Galactic plane because their signals are more strongly affected by propagation effects caused by the interstellar medium. We see however from Figure 9 that UL systems, which have the most rapidly spinning pulsars, are found at larger (projected) distances compared to those with He WDs. This is explained by the important increase in discoveries of high-$\dot{E}$ sources (i.e., very fast-spinning pulsars such as those with UL companions) by *Fermi*-LAT and targeted radio searches of *Fermi* sources over the past years (e.g., Abdo et al. 2009, 2010, 2013; Acero et al. 2015).

In addition to the bias toward nearby objects, a longitudinal asymmetry for binaries with low-mass companions is also observed. Unlike the expected latitudinal bias that results from the larger dispersive smearing and scattering near the plane, a binary-type dependence in the longitudinal distribution reflects different survey efficiencies. We interpret the skewness in (X,Y) position for He WD and UL binaries toward the PALFA-covered regions (shaded regions in Figure 9) as a survey bias: PALFA outperforms most surveys in discovering distant, very recycled pulsars. The observed population is consequently not representative of the true field population, and this should be taken into consideration in population modeling. Having sensitive surveys conducted at high frequencies capable of finding fast MSPs in the Galactic plane is therefore important for accurately modeling the population.
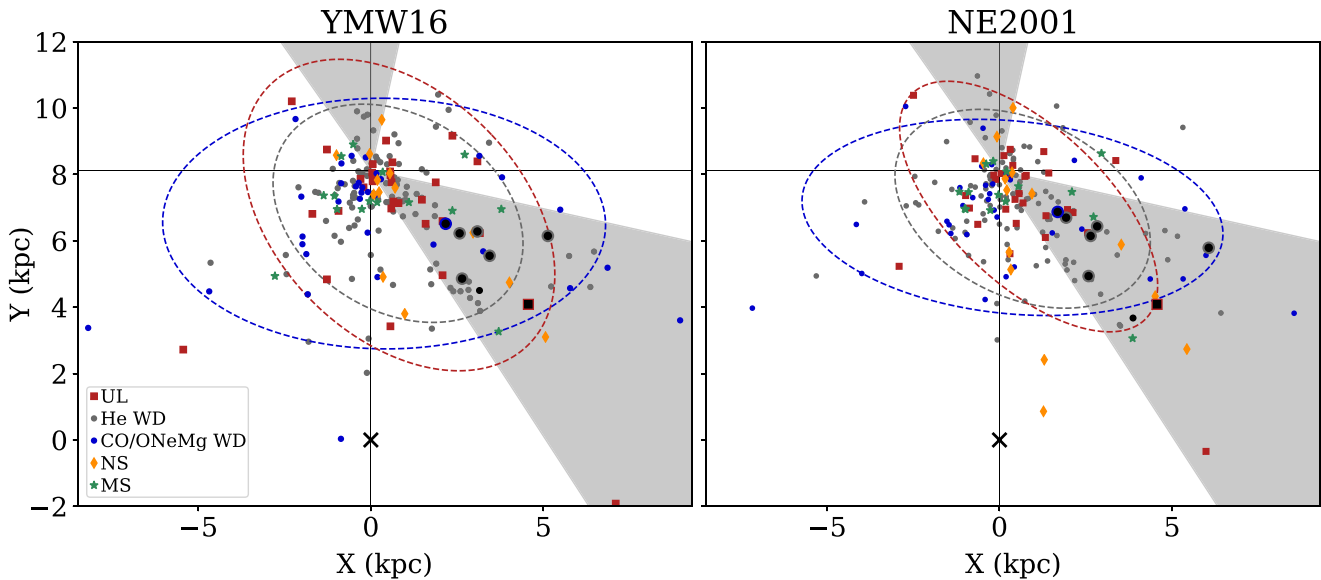
Figure 9. Spatial distribution of known binary MSPs in the X,Y,Z Cartesian coordinate system (based on the equatorial system) projected onto the X–Y Galactic plane using distance predictions from the YMW16 (left panel) and NE2001 (right panel) electron density models. Shaded sections are PALFA-covered regions, and the color-based classification for the binary type is the same as in Figure 7. MSPs presented in this work are represented by black-filled circles. The black X marker corresponds to the Galactic center, and the solar system barycenter is located at the intersection of the two solid black lines. Dashed ellipses are the 2σ fits to the X–Y Galactic coordinates for each binary class. Unlike the blue ellipse (CO/ONeMg WD companions), the semimajor axis of the red and gray ellipses (UL and He WD companions) are not parallel to the x-axis, indicative of an asymmetry about $X = 0$ kpc. This is due to the significant contribution of the PALFA survey to the known UL and He WD binaries.

4.2. Galactic Height

Kick velocities imparted to neutron stars following asymmetric supernova (SN) explosions strongly impact the Galactic height distribution of pulsars. In this event, overall momentum is conserved. But where for isolated pulsars the accelerated mass is only that of the neutron star, binary pulsars need to also drag along their companion. Due to this higher system mass, one theoretically expects the recoil velocity to be smaller for binary pulsars compared to isolated pulsars (e.g., Kiel & Hurley 2009), and to decrease with increasing companion mass. The Galactic height of observed pulsars belonging to various populations are used as probes in testing predictions emerging from simulations.

Additionally, performing such a comparison is relevant for estimating the contribution of pulsars to the unresolved diffuse γ-ray background, a long-standing open problem in astrophysics. Indeed, the γ-ray luminosity of a pulsar scales with spin-down power and is consequently greater for highly recycled pulsars with light companions (e.g., Abdo et al. 2013). Hence, assessing a representative height distribution for the different binary classes is highly motivated.

Ng et al. (2014) (hereafter N14) investigated the possible correlation between the mass function of MSP binaries in the Galactic field and their vertical distance from the Galactic plane. Their primary conclusions were that (1) more massive systems are found closer to the Galactic plane and (2) there is a larger scatter in the height distribution of lighter systems.

We reproduce this analysis using an updated and larger sample of 214 MSP binaries[27] in the field (versus 164 in N14), taken from the ATNF Catalogue and the Galactic MSP Catalog.[28] Similarly to N14, we adopt the Tauris et al. (2012)

prescription to classify systems with unspecified companion type.

Distance estimates were calculated with both the NE2001 and YMW16 electron density models, and we compare the resulting projected heights. For every binary class, YMW16 produces larger absolute mean heights, $|z_{mean}|$, and standard deviations in absolute heights σ (see Table 4) than NE2001. We note however that YMW16 predicts distances larger than NE2001 for only 55% of the pulsars, so the larger $|z_{mean}|$ values are not a consequence of systematic distance overestimations compared to NE2001. While NE2001 predicts that all pulsars are within 1.25 kpc from the Galactic plane, some systems could be found at heights as large as 2.50 kpc according to YMW16 predictions. In the latter model, pulsars having $|z| > 1.0$ kpc are distant, high-latitude ($|b| > 15°$) systems. In a recent study that used new parallax measurements, Deller et al. (2019) demonstrated that while YMW16 performs moderately better than NE2001 at high latitudes, predictions that were largely inconsistent with parallax measurements were mostly high-latitude objects. We therefore emphasize that interpretations from this analysis are subjected to significant uncertainties and should be considered with caution. Results for each binary classes are discussed below.

4.2.1. MSP–WD Binaries

When considering systems with WD companions, our results agree with and strengthen conclusion (2) of N14: lighter MSP–WD systems show more scatter in their Galactic height distribution than the massive ones. This is true for both electron density models. Compared to pulsars with CO/ONeMg WDs, those with UL companions have estimated $|z_{mean}|$ larger by factors of two and three based on the NE2001 and YMW16 models, respectively.

As mentioned in N14, while our ability to detect rapidly rotating MSPs (i.e., the more recycled, lighter systems) is

---

[27] Again, using the following definition of recycled pulsars: $P < 100$ ms and $\dot{P} < 1 \times 10^{-17}$.
[28] http://astro.phys.wvu.edu/GalacticMSPs/GalacticMSPs.txt

Table 4
Statistical Height Distributions for the Five Binary-MSP Classes, Summarizing Results Shown in Figure 10

Binary class	N	YMW16		NE2001	
		$|z_{mean}|$ (kpc)	σ (kpc)	$|z_{mean}|$ (kpc)	σ (kpc)
UL	31	0.72	0.54	0.51	0.23
He WD	118	0.42	0.46	0.34	0.24
CO/ONeMg WD	34	0.25	0.30	0.21	0.18
NS	14	0.33	0.38	0.27	0.27
MS	15	0.67	0.56	0.39	0.24

Note. N, $|z_{mean}|$ and σ are the number of systems, the mean absolute height and the corresponding standard deviation in $|z|$ for each binary class, respectively.

strongly reduced as we search regions of high electron density close to the disk, the detectability of less-recycled pulsars with massive WDs is not as height dependent because the typical timescales of pulse dispersion/scattering are smaller relative to the pulse widths of these longer-spin-period pulsars. MSPs with CO/ONeMg WDs are therefore easier to detect. Consequently, the observed lack of heavy systems far from the Galactic plane seems genuine and the mean absolute distance from the plane $|z_{mean}|$ (0.25 kpc for YMW16 and 0.21 kpc for NE2001) is most probably representative of the true population for this class.

As a result of stronger observational biases, the measured $|z_{mean}|$ (0.72 kpc for YMW16 and 0.51 kpc for NE2001) of the lighter MSP-UL systems is likely overestimated. Evidence for this is the $|z|$ distribution in Figure 10, which reveals an overdensity of objects at an absolute height of $\sim$0.8 kpc. The majority of those MSPs have been recently discovered via *Fermi*-directed searches (Ray et al. 2012). Considering the higher detection threshold at low Galactic latitude of *Fermi*-LAT due to the higher background diffuse emission (Acero et al. 2015), we can extrapolate from those overdensities and predict a larger population near the Galactic plane.

N14 noted that pulsar ages could influence the observed scatter in heights: fully recycled pulsars with lower-mass companions are generally older than those with massive companions, resulting in lighter systems having more time to move away from the Galactic plane. We know however that in and out-of-the-plane oscillatory motions of neutron stars (having velocities smaller than the Galaxy's escape velocity) in response to the Galactic gravitational field have periods of the order of 10^7 yr (Cordes & Chernoff 1998), much shorter than the age of MSPs. Current scale heights could however be affected by the age of the MSP due to the different scale heights at birth associated to system progenitors as well as timescales associated to gravitational diffusion processes (Cordes & Chernoff 1998). Consequently, the larger scatter in scale heights for lower-mass-function systems is most likely a result of correlations between binary mass function, systemic recoil velocity, SN processes, birth scale height distribution and Galactic diffusion.

We also notice a mild deficiency of systems with CO or ONeMg WDs having mass function between $\sim$4 × 10^{-2} and 9 × 10^{-2} $M_\odot$ in the top panel of Figure 10 (indicated by a blue arrow), resulting in two possible subpopulations. Approximately 40% of our sample of MSP-CO/ONeMg WD binaries falls below this apparent gap. To determine if the observed

mass functions could originate from a uniform distribution, we generated trial samples and performed a two-sided Kolmogorov–Smirnov tests. The samples shared the same mass function interval as the observed sample and were of the same size. To avoid fluctuations due to small number statistics, we generated 10,000 trial samples. The average probability that the observed and trial samples share a common parent distribution is 3%, suggesting that the MSP-CO/ONeMg mass functions are not drawn from a uniform distribution.

The known orbital period gap at $P_b \sim$ 25–50 days (e.g., Tauris 1996; Taam et al. 2000; Hui et al. 2018) that possibly arises from a bifurcation mechanism leading to divergent evolutionary paths (Tauris 1996) does not explain this apparent population splitting: members of these subpopulations are found on both sides of this P_b gap. We note here that two of the pulsars presented in this work, PSRs J1921+1929 and J1932 +1756, fall within this period gap. Furthermore, the fraction of higher-mass-function systems seems too high to be explained by systems where the companions are the more massive ONeMg WDs, which are rarer than the lighter CO WDs. An alternative interpretation is an asymmetry in mass ratios, possibly reflecting the asymmetric distribution of the NS masses found by previous studies (Valentim et al. 2011; Özel et al. 2012; Kiziltan et al. 2013; Antoniadis et al. 2016). Further discoveries will help in confirming the existence of this possible gap within MSP-massive WD binaries.

4.2.2. MSP–NS Binaries

Because DNSs endure two SN kicks rather than one, DNS heights are not interpreted in the same manner as those involving WD companions. From Figure 10, we note that there seems to be a bimodality in the Galactic heights for the YMW16 estimations, uncorrelated with the mass function, in which 10 DNSs have $|z| < 0.25$ kpc and the remaining four have $|z|$ between 0.75 and 1.1 kpc. This potential separation in the observed population is however not as significant in the NE2001 predictions. If real, this could be related to the bimodal natal kick distributions that arise from the different SN mechanisms giving birth to the NSs (e.g., Schwab et al. 2010; Andrews et al. 2015; Beniamini & Piran 2016; Vigna-Gómez et al. 2018).

Prior to the second SN, all future DNS systems are completely circularized, as a result of the accretion process. When the second SN occurs, the magnitude and direction of the associated kick and the SN mass loss determine the post-SN orbital eccentricity and the system's velocity relative to the Galaxy: the larger the kick, the larger (on average) will be the post-SN orbital eccentricities and motions relative to the Galaxy. A positive correlation between these quantities has indeed been detected (Tauris et al. 2017).

Thus the systems with low orbital eccentricity ($e < 0.15$) and low peculiar velocity, which likely had a small kick (e.g., PSRs J0453+1559; Martinez et al. 2017, J0737−3039A/B; Burgay et al. 2003; Lyne et al. 2004, J1906+0746; van Leeuwen et al. 2015, J1913+1102; Lazarus et al. 2016, J1946+2052; Stovall et al. 2018) should always be located near the Galactic plane; this is indeed observed: their maximum Galactic height is about 0.3 kpc. Broader distributions of orbital periods, eccentricities, and systemic velocities are expected for systems with large-kick second SNe (Dewi et al. 2005). For $e > 0.15$, the range of Galactic heights implied by the YMW16 model increases to 1.2 kpc; all high-altitude ($z > 0.7$ kpc) systems (PSRs B1534
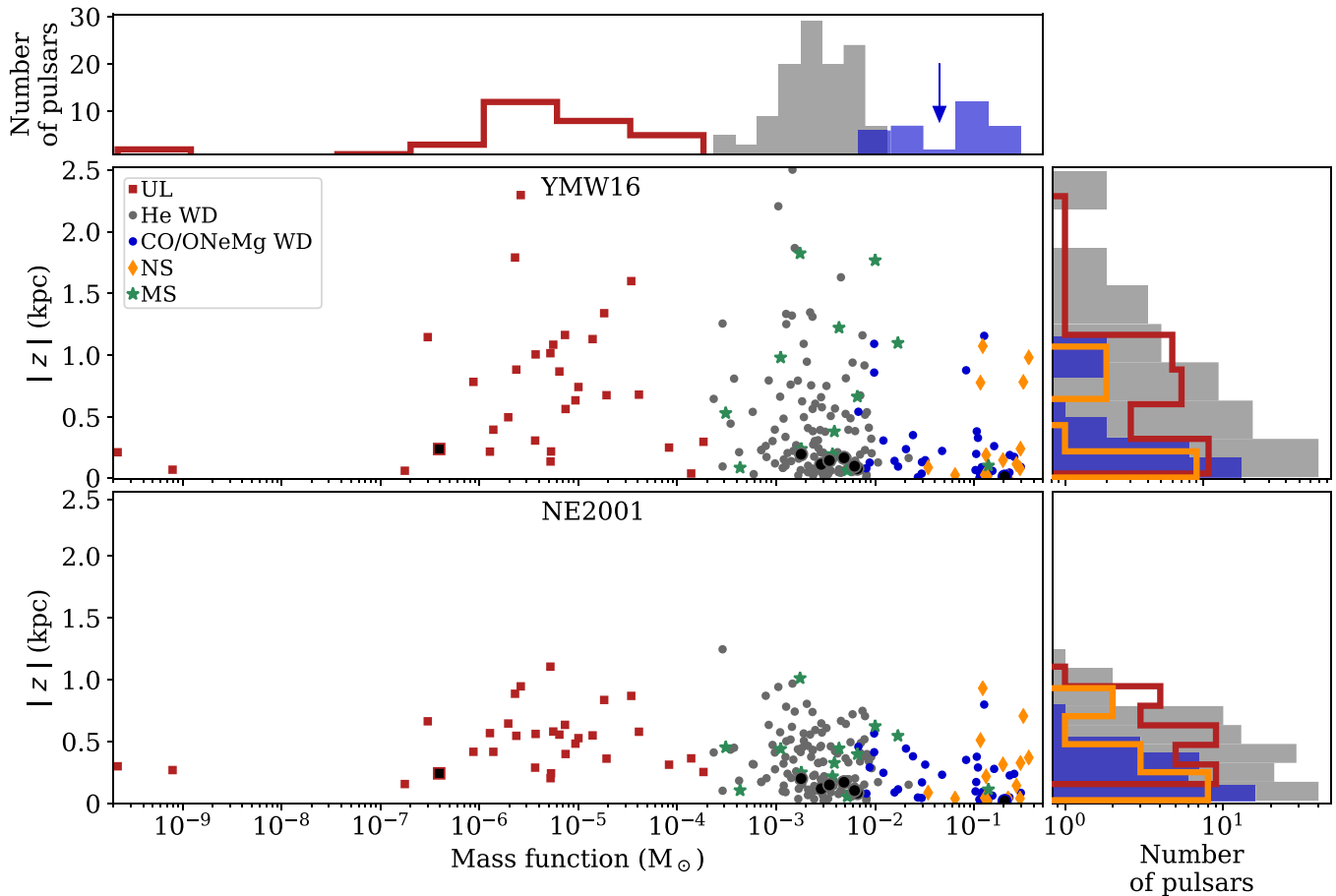
Figure 10. Bottom left panel: absolute Galactic height |z| vs. mass function of Galactic MSPs in binary systems. Black-filled symbols are the MSPs presented in this work. Top panel: mass function distributions for systems with UL, He WD, and CO/ONeMg WD companions. The blue arrow points to the gap in mass functions of MSP–CO/ONeMg WD binaries we discuss in Section 4.2.1. To help visualize this gap more clearly, histograms for MSP–NS and MSP–MS mass functions are not plotted on this panel. Right panel: height distributions for those same binary categories. Overdensities of UL and He WD binaries at |z| ~ 1 kpc are the result of the increasing number of *Fermi*-directed radio discoveries. Also for clarity, we do not plot the heights of MSP–MS systems.

+12; Wolszczan 1991, J1518+4904; Nice et al. 1996, J1411 +2551; Martinez et al. 2017, J1757−1854; Cameron et al. 2018) have $e > 0.15$. Those pulsars also have the highest |z| values implied by NE2001, but their range in |z| only extends from 0.37–0.93 kpc away from the plane. We note that a distance measurement based on the orbital decay of PSR B1534+12 (Stairs et al. 1998; Fonseca et al. 2014) was used as a predictor while constructing both electron density models, therefore the measured Galactic height for this source is DM independent.

It will be important to see if future discoveries confirm the significance of this potential gap in DNS heights. This type of study will enable increasingly accurate models of massive stellar binary evolution and SN kick distributions.

4.2.3. MSP–MS Binaries

Galactic, recycled pulsars in orbit with low-mass, hydrogen-rich (likely nondegenerate) stars are difficult to detect. This is a consequence of radio eclipses caused by the stellar material surrounding the system. Those are referred to as "redback" systems (Roberts 2013), and only 14 have been confirmed as such (see recent work by Strader et al. 2019). The 15 MSP–MS binaries in our sample have MSPs with $P < 8$ ms and DM < 70 pc cm^{-3}, except PSR J1903+0327, a unique PALFA discovery. The latter system has a DM of 298 pc cm^{-3} and is in

an eccentric orbit ($e = 0.44$, Champion et al. 2008) with a star of spectral type between F5V and G0V (Freire et al. 2011; Khargharia et al. 2012). It is the only member of our sample that is not a redback.

From Figure 10 and Table 4, we see that systems with MS stars have mass functions, $|z_{mean}|$ and σ values similar to those with WDs ($M_{WD} \gtrsim 0.1 M_\odot$): a large scatter in both their heights and mass functions. Similarly to MSPs with UL/He WD companions, their short spin periods make them harder to detect because of interstellar dispersion and scattering. In recent years, redbacks have been largely discovered via targeted searches of *Fermi* unassociated sources (e.g., Hessels et al. 2011; Cromartie et al. 2016), which also has a reduced detection capability close to the disk (Acero et al. 2015). Thus, the same observational bias against near-the-plane discoveries applies and we conclude that $|z_{mean}|$ is likely overestimated for this binary class as well.

5. Summary and Conclusion

Timing solutions for eight new PALFA-discovered MSPs in binary systems were presented in this work. All follow-up observations were conducted at 1.4 GHz at AO and JBO.

Among the discoveries are (1) a black widow pulsar (PSR J1928+1245) for which we do not detect eclipses, (2) a new γ-ray MSP (PSR J1921+1929) that we associate with a *Fermi*

point source, and (3) an intermediate-mass binary pulsar (PSR J1932+1756) in a low-eccentricity orbit with a massive WD. Seven of the new discoveries are very fast-spinning ($P < 6$ ms), binary MSPs deep in the Galactic plane, which are particularly difficult to detect as a result of pulse dispersion and scattering by the dense interstellar medium. Most systems are in nearly circular orbits in which the most probable companions are He WDs. Except for γ-ray pulsations from PSR J1921+1929, we do not detect any other multiwavelength counterparts or possible associations to the pulsars.

In this work, we also analyzed the Galactic distribution of 214 recycled pulsars belonging to different binary classes. We see that MSPs with massive WDs show less scatter in their absolute Galactic heights compared to lighter systems, in agreement with results from Ng et al. (2014). MSP-CO/ONeMg WD binaries being less vulnerable to observational biases, we believe that our measured average heights, $|z_{\mathrm{mean}}|$, of 0.25 and 0.21 kpc for the YMW16 and NE2001 electron density models, respectively, are more representative of the true population than MSPs in orbit with lighter WDs.

We identify a longitudinal bias for finding the most recycled MSP binaries toward PALFA-covered regions, and an overdensity of such objects at $|z| \sim 0.8$ kpc, which reflects the increased number of discoveries from *Fermi*-directed radio searches. Those are indications that we are starting to unveil a more representative population near the plane. However, PALFA only surveys regions at $|b| < 5°$. This itself represents an important selection bias. Without searching regions of higher Galactic latitude with surveys having PALFA-like sensitivity, a sample more representative of the true population cannot be produced.

A potential gap in the mass function of systems with massive WDs at $\sim 4 \times 10^{-2}$–9×10^{-2} $M_\odot$ is found, potentially reflecting a bimodal distribution in binary mass ratios.

Additionally, distances estimated with the YMW16 model suggest a potential gap, uncorrelated with eccentricity, in the absolute heights of the 14 known DNSs in the Galactic field at approximately $250 \lesssim |z| \lesssim 750$ pc. If this gap persists as more systems are discovered, we could gain new information on the SN mechanisms producing those DNSs.

The new PALFA discoveries presented in this work belong to this population of faint, high-DM MSPs, and the non-detection of high-energy pulsations for all but one of those new pulsars indicates that PALFA is complementary to the ongoing survey with *Fermi*. Further discoveries from the survey will continue to unveil a more complete census of the Galactic MSP population in the plane.

ORCID iDs

E. Parent ● https://orcid.org/0000-0002-0430-6504
V. M. Kaspi ● https://orcid.org/0000-0001-9345-0307
S. M. Ransom ● https://orcid.org/0000-0001-5799-9714
P. C. C. Freire ● https://orcid.org/0000-0003-1307-9435
F. Camilo ● https://orcid.org/0000-0002-1873-3718
S. Chatterjee ● https://orcid.org/0000-0002-2878-1502
J. M. Cordes ● https://orcid.org/0000-0002-4049-1882
F. Crawford ● https://orcid.org/0000-0002-2578-0360
J. S. Deneva ● https://orcid.org/0000-0003-1226-0793
R. D. Ferdman ● https://orcid.org/0000-0002-2223-1235
J. W. T. Hessels ● https://orcid.org/0000-0003-2317-1446
M. A. McLaughlin ● https://orcid.org/0000-0001-7697-7422
P. Scholz ● https://orcid.org/0000-0002-7374-7119
I. H. Stairs ● https://orcid.org/0000-0001-9784-8670
W. W. Zhu ● https://orcid.org/0000-0001-5105-4058

References

Abdo, A. A., Ackermann, M., Ajello, M., et al. 2009, Sci, 325, 840
Abdo, A. A., Ackermann, M., Ajello, M., et al. 2010, ApJS, 187, 460
Abdo, A. A., Ajello, M., Allafort, A., et al. 2013, ApJS, 208, 17
Abbott, B. P., Abbott, R., Adhikari, R., et al. 2009, RPPh, 72, 076901
Acero, F., Ackermann, M., Ajello, M., et al. 2015, ApJS, 218, 23
Alpar, M. A., Cheng, A. F., Ruderman, M. A., & Shaham, J. 1982, Natur, 300, 728
Andrews, J. J., Farr, W. M., Kalogera, V., & Willems, B. 2015, ApJ, 801, 32
Antoniadis, J., Tauris, T. M., Ozel, F., et al. 2016, ApJ, submitted (arXiv:1605.01665)
Arzoumanian, Z., Brazier, A., Burke-Spolaor, S., et al. 2018, ApJS, 235, 37
Beniamini, P., & Piran, T. 2016, MNRAS, 456, 4089
Bhattacharya, D., & van den Heuvel, E. P. J. 1991, PhR, 203, 1
Boller, T., Freyberg, M. J., Trümper, J., et al. 2016, A&A, 588, A103

Burgay, M., D'Amico, N., Possenti, A., et al. 2003, Natur, 426, 531
Cameron, A. D., Champion, D. J., Kramer, M., et al. 2018, MNRAS, 475, L57
Camilo, F., Lyne, A. G., Manchester, R. N., et al. 2001, ApJL, 548, L187
Champion, D. J., Ransom, S. M., Lazarus, P., et al. 2008, Sci, 320, 1309
Coifman, R. R., & Donoho, D. L. 1995, Translation-Invariant De-Noising (New York: Springer New York), 125
Cordes, J. M., & Chernoff, D. F. 1998, ApJ, 505, 315
Cordes, J. M., Freire, P. C. C., Lorimer, D. R., et al. 2006, ApJ, 637, 446
Cordes, J. M., & Lazio, T. J. W. 2002, arXiv:astro-ph/0207156
Cordes, J. M., Weisberg, J. M., & Boriakoff, V. 1985, ApJ, 288, 221
Crawford, F., Stovall, K., Lyne, A. G., et al. 2012, ApJ, 757, 90
Cromartie, H. T., Camilo, F., Kerr, M., et al. 2016, ApJ, 819, 34
Damour, T., & Deruelle, N. 1986, AIHS, 44, 263
Damour, T., & Taylor, J. H. 1991, ApJ, 366, 501
de Jager, O. C., & Büsching, I. 2010, A&A, 517, L9
Deller, A. T., Goss, W. M., Brisken, W. F., et al. 2019, ApJ, 875, 100
Demorest, P. B., Ferdman, R. D., Gonzalez, M. E., et al. 2013, ApJ, 762, 94
Deneva, J. S., Freire, P. C. C., Cordes, J. M., et al. 2012, ApJ, 757, 89
Dewi, J. D. M., Podsiadlowski, P., & Pols, O. R. 2005, MNRAS, 363, L71
Eichler, D., & Levinson, A. 1988, ApJL, 335, L67
Fonseca, E., Stairs, I. H., & Thorsett, S. E. 2014, ApJ, 787, 82
Foster, R. S., & Backer, D. C 1990, ApJ, 361, 300
Freire, P. C. C. 2005, in ASP Conf. Ser. 328, Binary Radio Pulsars, ed. F. A. Rasio & I. H. Stairs (San Francisco, CA: ASP), 405
Freire, P. C. C., Bassa, C. G., Wex, N., et al. 2011, MNRAS, 412, 2763
Freire, P. C. C., & Ridolfi, A. 2018, MNRAS, 476, 4794
Fruchter, A. S., Berman, G., Bower, G., et al. 1990, ApJ, 351, 642
Gaia Collaboration, Clementini, G., Eyer, L., et al. 2017, A&A, 605, A79
Gentile, P. A., McLaughlin, M. A., Demorest, P. B., et al. 2018, ApJ, 862, 47
Guillemot, L., Octau, F., Cognard, I., et al. 2019, A&A, 629, 92
Hellings, R. W., & Downs, G. S. 1983, ApJL, 265, L39
Hessels, J. W. T., Roberts, M. S. E., McLaughlin, M. A., et al. 2011, in AIP Conf. Ser. 1357, Radio Pulsars: An Astrophysical Key to Unlock the Secrets of the Universe, ed. M. Burgay (Melville, NY: AIP), 40
Hobbs, G., Archibald, A., Arzoumanian, Z., et al. 2010, CQGra, 27, 084013
Hotan, A. W., van Straten, W., & Manchester, R. N. 2004, PASA, 21, 302
Hui, C. Y., Wu, K., Han, Q., Kong, A. K. H., & Tam, P. H. T. 2018, ApJ, 864, 30
Jaffe, A. H., & Backer, D. C. 2003, ApJ, 583, 616
Khargharia, J., Stocke, J. T., Froning, C. S., Gopakumar, A., & Joshi, B. C. 2012, ApJ, 744, 183
Kiel, P. D., & Hurley, J. R. 2009, MNRAS, 395, 2326
Kiziltan, B., Kottas, A., Yoreo, M. D., & Thorsett, S. E. 2013, ApJ, 778, 66
Knispel, B., Lyne, A. G., Stappers, B. W., et al. 2015, ApJ, 806, 140
Lange, C., Camilo, F., Wex, N., et al. 2001, MNRAS, 326, 274
Lazaridis, K., Wex, N., Jessner, A., et al. 2009, MNRAS, 400, 805
Lazarus, P., Brazier, A., Hessels, J. W. T., et al. 2015, ApJ, 812, 81
Lazarus, P., Freire, P. C. C., Allen, B., et al. 2016, ApJ, 831, 150
Lorimer, D. R., Stairs, I. H., Freire, P. C., et al. 2006, ApJ, 640, 428
Lyne, A. G., Burgay, M., Kramer, M., et al. 2004, Sci, 303, 1153
Manchester, R. N. 2017, JApA, 38, 42
Manchester, R. N., Hobbs, G. B., Teoh, A., & Hobbs, M. 2005, yCat, 7245
Martinez, J. G., Stovall, K., Freire, P. C. C., et al. 2017, ApJL, 851, L29
Ng, C., Bailes, M., Bates, S. D., et al. 2014, MNRAS, 439, 1865
Nice, D. J., Sayer, R. W., & Taylor, J. H. 1996, ApJL, 466, L87
Nice, D. J., & Taylor, J. H. 1995, ApJ, 441, 429
Özel, F., Psaltis, D., Narayan, R., & Villarreal, A. S. 2012, ApJ, 757, 55
Parent, E., Kaspi, V. M., Ransom, S. M., et al. 2018, ApJ, 861, 44
Patel, C., Agarwal, D., Bhardwaj, M., et al. 2018, ApJ, 869, 181
Phinney, E. S. 1992, RSPTA, 341, 39
Radhakrishnan, V., & Srinivasan, G. 1982, CSci, 51, 1096
Ransom, S. M. 2001, PhD thesis, Harvard Univ.
Ray, P. S., Abdo, A. A., Parent, D., et al. 2012, arXiv:1205.3089
Reid, M. J., Menten, K. M., Brunthaler, A., et al. 2014, ApJ, 783, 130
Rickett, B. J., Coles, W. A., & Bourgois, G. 1984, A&A, 134, 390
Roberts, M. S. E. 2013, in IAU Symp. 291, Neutron Stars and Pulsars: Challenges and Opportunities after 80 years, ed. J. van Leeuwen (Cambridge: Cambridge Univ. Press), 127
Saxton, R. D., Read, A. M., Esquej, P., et al. 2008, A&A, 480, 611
Scheuer, P. A. G. 1968, Natur, 218, 920
Scholz, P., Kaspi, V. M., Lyne, A. G., et al. 2015, ApJ, 800, 123
Schwab, J., Podsiadlowski, P., & Rappaport, S. 2010, ApJ, 719, 722
Shklovskii, I. S. 1970, SvA, 13, 562
Sieber, W. 1982, A&A, 113, 311
Siemens, X., Ellis, J., Jenet, F., & Romano, J. D. 2013, CQGra, 30, 224015
Skrutskie, M. F., Cutri, R. M., Stiening, R., et al. 2006, AJ, 131, 1163
Smith, D. A., Bruel, P., Cognard, I., et al. 2019, ApJ, 871, 78
Stairs, I. H., Arzoumanian, Z., Camilo, F., et al. 1998, ApJ, 505, 352
Stinebring, D. R., & Condon, J. J. 1990, ApJ, 352, 207
Stovall, K. 2013, PhD thesis, Univ. Texas at San Antonio
Stovall, K., Allen, B., Bogdanov, S., et al. 2016, ApJ, 833, 192
Stovall, K., Freire, P. C. C., Chatterjee, S., et al. 2018, ApJL, 854, L22
Strader, J., Swihart, S. J., Chomiuk, L., et al. 2019, ApJ, 872, 42
Sugizaki, M., Mitsuda, K., Kaneda, H., et al. 2001, ApJS, 134, 77
Taam, R. E., King, A. R., & Ritter, H. 2000, ApJ, 541, 329
Tauris, T. M. 1996, A&A, 315, 453
Tauris, T. M., Kramer, M., Freire, P. C. C., et al. 2017, ApJ, 846, 170
Tauris, T. M., Langer, N., & Kramer, M. 2012, MNRAS, 425, 1601
Tauris, T. M., & Savonije, G. J. 1999, A&A, 350, 928
Tauris, T. M., van den Heuvel, E. P. J., & Savonije, G. J. 2000, ApJL, 530, L93
Taylor, J. H. 1992, RSPTA, 341, 117
Taylor, J. H., Fowler, L. A., & McCulloch, P. M. 1979, Natur, 277, 437
The NANOGrav Collaboration, Arzoumanian, Z., Brazier, A., et al. 2015, ApJ, 813, 65
Valentim, R., Rangel, E., & Horvath, J. E. 2011, MNRAS, 414, 1427
van Leeuwen, J., Kasian, L., Stairs, I. H., et al. 2015, ApJ, 798, 118
Vigna-Gómez, A., Neijssel, C. J., Stevenson, S., et al. 2018, MNRAS, 481, 4009
Wang, S., Liu, J., Qiu, Y., et al. 2016, ApJS, 224, 40
Wolszczan, A. 1991, Natur, 350, 688
Yao, J. M., Manchester, R. N., & Wang, N. 2017, ApJ, 835, 29